Proteomic and Metabolomic Characterization of COVID-19 Patient Sera

Bo Shen[1#], Xiao Yi[2,3#], Yaoting Sun[2,3#], Xiaojie Bi[1#], Juping Du[1#], Chao Zhang[4#], Sheng Quan[4#], Fangfei Zhang[2,3], Rui Sun[2,3], Liujia Qian[2,3], Weigang Ge[2,3], Wei Liu[2,3], Shuang Liang[2,3], Hao Chen[2,3], Ying Zhang[1], Jun Li[1], Jiaqin Xu[1], Zebao He[1], Baofu Chen[1], Jing Wang[1], Haixi Yan[1], Yufen Zheng[1], Donglian Wang[1], Jiansheng Zhu[1], Ziqing Kong[4], Zhouyang Kang[4], Xiao Liang[2,3], Xuan Ding[2,3], Guan Ruan[2,3], Nan Xiang[2,3], Xue Cai[2,3], Huanhuan Gao[2,3], Lu Li[2,3], Sainan Li[2,3], Qi Xiao[2,3], Tian Lu[2,3], Yi Zhu[2,3*], Huafen Liu [4*], Haixiao Chen[1*], Tiannan Guo[2,3,5*]

[1]Taizhou Hospital, Wenzhou Medical University, 150 Ximen Street, Linhai 317000, Zhejiang Province, China;

[2]Key Laboratory of Structural Biology of Zhejiang Province, School of Life Sciences, Westlake University, 18 Shilongshan Road, Hangzhou 310024, Zhejiang Province, China;

[3]Institute of Basic Medical Sciences, Westlake Institute for Advanced Study, 18 Shilongshan Road, Hangzhou 310024, Zhejiang Province, China;

[4]Calibra Lab at DIAN Diagnostics, 329 Jinpeng Street, Hangzhou 310030, Zhejiang Province, China;

[5]Lead Contact

co-first;

* Correspondence: zhuyi@westlake.edu.cn (Y.Z.); liuhf1@dazd.cn (H.L.); chenhx@enzemed.com (H.C.); guotiannan@westlake.edu.cn (T.G.)

SUMMARY

Severe COVID-19 patients account for most of the mortality of this disease. Early detection and effective treatment of severe patients remain major challenges. Here, we performed proteomic and metabolomic profiling of sera from 46 COVID-19 and 53 control individuals. We then trained a machine learning model using proteomic and metabolomic measurements from a training cohort of 18 non-severe and 13 severe patients. The model correctly classified severe patients with an accuracy of 93.5%, and was further validated using ten independent patients, seven of which were correctly classified. We identified molecular changes in the sera of COVID-19 patients implicating dysregulation of macrophage, platelet degranulation and complement system pathways, and massive metabolic suppression. This study shows that it is possible to predict progression to severe COVID-19 disease using serum protein and metabolite biomarkers. Our data also uncovered molecular pathophysiology of COVID-19 with potential for developing anti-viral therapies.

INTRODUCTION

Coronavirus disease 2019 (COVID-19) is an unprecedented global threat caused by severe acute respiratory syndrome coronavirus 2 (SARS-CoV-2). It is currently spreading around the world rapidly. The sudden outbreak and accelerated spreading of SARS-CoV-2 infection have caused substantial public concerns. Within about two months, close to one million individuals worldwide have been infected, leading to about 50,000 deaths. At the time of writing this manuscript, about 100,000 new infections are reported daily.

Most COVID-19 studies have focused on its epidemiological and clinical characteristics(Ghinai et al., 2020; Guan et al., 2020; Li et al., 2020b; Team, 2020). About 80% of patients infected with SARS-CoV-2 displayed mild symptoms with good prognosis(Team, 2020). They usually recover with, or even without, conventional medical treatment, and therefore are classified as mild or moderate COVID-19 (Medicine, 2020; Thevarajan et al., 2020). However, about 20% of patients suffer from respiratory distress and require immediate oxygen therapy or other inpatient interventions, including mechanical ventilation (Medicine, 2020; Murthy et al., 2020; Wu and McGoogan, 2020). These patients, classified as clinically severe or critical life-threatening infections, are mainly diagnosed empirically based on a set of clinical characteristics, such as respiratory rate (≥ 30 times/min), mean oxygen saturation (≤ 93% in the resting state) or arterial blood oxygen partial pressure/oxygen concentration (≤ 300 mmHg) (Medicine, 2020). However, patients exhibiting these clinical manifestations have already progressed to a clinically severe phase and require immediate access to specialized intensive care; otherwise, they may die rapidly. Therefore, it is critical to develop new approaches to predict early which cases will likely become clinically severe. In addition, effective therapy for severe patients remains speculative, largely due to limited understanding of SARS-CoV-2 pathogenesis.

In this study, we hypothesized that SARS-CoV-2 induces characteristic molecular changes that can be detected in the sera of severe patients. These molecular changes may shed light on therapy development for COVID-19 patients. To test this hypothesis, we applied cutting-edge proteomic (Aebersold and Mann, 2016; Li et al., 2020a) and metabolomic (Hou et al., 2020; Lee et al., 2019) technologies to analyze the proteome and metabolome of sera from severe COVID-19 patients and several control groups.

RESULTS

Proteomic and metabolomic profiling of COVID-19 sera

We procured a cohort of patients (Zheng et al., 2020) containing 21 severe COVID-19 patients, in which 11 sera from severe patients were collected one to six days before the patients were clinically assessed as

severe. Sera from the remaining eight patients were collected within about 3 days after diagnosed as severe cases (Figure 1A, Table 1, Table S1). Controls with matched epidemiological features were included to identify severity-related molecular alterations. These controls were 28 healthy subjects, 25 non-COVID-19 patients (negative for the SARS-CoV-2 nucleic acid test) with similar clinical characteristics as COVID-19 patients, and 25 non-severe COVID-19 patients. A serum sample was obtained from each patient within a few days after hospital admission, with a few exceptions when samplings were performed at later disease stages.

We used stable isotope labeled proteomics strategy TMTpro (16plex) (Li et al., 2020a) and UPLC-MS/MS untargeted metabolomics approach to analyze 92 undepleted sera from 86 individuals. Altogether 894 proteins were quantified and 941 (including 36 drugs and their metabolites) metabolites were identified with authentic compound library searching. For metabolomic analysis, both hydrophilic and hydrophobic molecules were analyzed using both positive and negative ionization to cover various endogenous biochemical classes. Our data were acquired with high degree of consistency and reproducibility. In quality control analysis, the median coefficient of variance (CV) values for proteomic and metabolomic data were 10% and 5%, respectively (Figure S1A). Remarkably, sera from SARS-CoV-2 infected patients were well resolved from healthy individuals, and the sera from severe patients displayed distinct proteomic and metabolomic patterns compared to those from other groups (Figures S1B-C).

Identification of severe patients using machine learning

We next investigated the possibility of classify the severe COVID-19 patients based on the molecular signatures of proteins and metabolites (Table S2). We built a random forest machine learning model based on proteomic and metabolomic data from 18 non-severe and 13 severe patients (Figure 1B), leading to prioritization of 29 important variables including 22 proteins and 7 metabolites (Figure 2A-B). This model reached an AUC of 0.957 in the training set (Figure 2C). One non-severe patient, XG3, was incorrectly classified as severe (Figure 2D), possibly because this 70-year-old male patient was the oldest individual in this cohort (Figure 1A). For patient XG40, the reason of incorrectly classified is unclear.

We then tested the model on an independent cohort of ten patients (Figure 2E, Table S3). All severe patients were correctly identified, except one patient, XG45, a 62-year-old male who had received traditional Chinese medicines during more than 20 days before admission. This individual was the patient with the longest pre-admission treatment in this cohort and the administration of traditional Chinese medicines might have also accounted for the incorrect prediction. Another incorrectly classified non-severe patient was XG22, a 43 year-old male with chronic HBV infection and diabetes who had the longest hospitalization (>50 days) among all non-severe patients. Indeed,

our molecular-based prediction flagged him as an outlier, suggesting that his prolonged treatment history might have interfered with the expression of the panel of the 29 variables. For reasons yet unclear, XG25, a 43-year-old male non-severe case, was incorrectly classified as severe.

Proteomic and metabolomic changes in severe COVID-19 sera

We found that 105 proteins were differentially expressed in COVID-19 patients, but not in the non-COVID-19 patients (Figure S2, S4). After correlating their expression with clinical disease severity (Figure S5), 93 proteins showed specific modulation in severe patients. Pathway analysis and network enrichment analyses of the 93 differentially expressed proteins revealed three pathways (Figure S6), namely activation of the complement system, macrophage function and platelet degranulation, involving 50 proteins (Figure 3A) in the sera of severe patients. Similarity, 373 and 204 metabolites were found with differential abundance in COVID-19 patients and continually changed correlated with disease severity in our metabolomics data, respectively (Figure S3, S4). Correspondingly, 82 metabolites were involved in the three biological processes. We summarize the key dysregulated molecules in Figure 5 and discussed in the following sections.

Dysregulated macrophage and lipid metabolism

Our data uncovered dysregulation of multiple apolipoproteins including APOA1, APOA2, APOH, APOL1, APOD and APOM (Figure 3A). Most of them are associated with macrophage function and were down-regulated. Decrease of APOA1 in serum has been reported during the transition of COVID-19 patients from mild to severe illness (Nie et al., 2020). The APOM in serum of severe patients was downregulated compared with healthy and non-severe COVID-19 patients. Regulation of serum APOM has also been observed in hepatitis B virus (HBV) patients (Gu et al., 2011).

Consistent with these proteomic findings, we also detected dysregulated metabolites involved in lipid metabolism. Accumulation of 16 steroid hormones in COVID-19 patients may contribute to macrophage modulation. Steroid hormones, including progesterone, androgens, estrogens and bile acids can promote the activity of macrophages (Vernon-Roberts, 1969). Specifically, glucocorticoids were recently reported to be clinically efficacious (Wang et al., 2020b). We detected increased 21-hydroxypregnenolone, the essential intermediate for synthesizing corticosterone, suggesting that corticosterone biosynthesis may be a protective mechanism against SARS-CoV-2 infection.

We also found evidence of significant activation of the kynurenine pathway. Metabolites of kynurenate, kynurenine, 8-methoxykynurenate were enriched in COVID-19 patients. Nicotinamide adenine dinucleotide (NAD+), the cofactor in many cellular redox reactions, can be synthesized from tryptophan by the kynurenine pathway and operates as a switch for macrophage effector responses (Minhas et al., 2019).

The macrophage process is closely related to lipid metabolism. Over 100 lipids were down-regualted in severe patients. Our data showed decreased sphingolipids in both non-severe and severe COVID-19 patients (Figure 4A). Sphingolipids and glycerophospholipids are important components of biomembranes, which mediate signal transduction and immune activation processes. Sphingolipids, such as sphingosine-1-phosphate, can induce macrophage activation, inhibit macrophage apoptosis, and promote migration of macrophages to inflammatory sites (Weigert et al., 2009). Phagocytosis and platelet degranulation are coupled with changes in biomembrane lipid composition and fluidity, and modulate the production of glycerophospholipids (Rouzer et al., 2007). In this study, we found continuous decrease of glycerophospholipids after SARS-CoV-2 infection. Glycerophospholipids and fatty acids such as arachidonic acid have been found significantly elevated in HCoV-229E-infected cells, and exogenous supplement of arachidonic acid significantly suppressed HCoV-229E and MERS-CoV replication (Yan et al., 2019). Our data suggest severe COVID-19 patients might benefit from this therapeutical strategy as well.

Choline and its derivatives were down-regulated in COVID-19 patients, particularly in severe cases; phosphocholine, the intermediate product for producing phosphatidylcholine (PC) was up-regulated (Figure 4B). This was probably due to activated macrophage-mediated immunity (Sanchez-Lopez et al., 2019). Polarization of macrophages in response to pathogens requires increased absorption of choline for PC formation, thereby promoting cytokine secretion (Sanchez-Lopez et al., 2019).

Activated acute phase proteins (APPs) and the complement system

We detected 10 APPs among 20 proteins that are differentially expressed between non-severe and severe groups (Figure 2A). They are involved at the early stages of immune responses to virus infection. Among the most significantly upregulated in severe sera were APPs, including serum amyloid A-1 (SAA1), serum amyloid A-2 (SAA2), serum amyloid A-4 (SAA4), C-reactive protein (CRP), alpha-1-antichymotrypsin (SERPINA3) and serum amyloid P-component (SAP/APCS) (Figure 3B). Some of them are known to be biomarkers for viral infections, including SAA1, SAA2 and CRP. While CRP has been associated with COVID-19, the other proteins have not previously been reported in COVID-19 (Liang et al., 2020). SAA1 was reported to be elevated in severe SARS patients, but was not specific to SARC-CoV (Pang et al., 2006). As a major contributor to acute phase response, complement system plays a crucial role in eliminating invading pathogens in the early stage of infection. Among those APPs, two proteins belong to the complement membrane attack complex, including complement 6 (C6) and complement factor B (CFB). Two other proteins, Properdin (CFP) and Carboxypeptidase N catalytic chain (CPN1), are regulators of complement system (Figure 3).

We also observed an accumulation of mannose and its derivatives in severe patients. In the complement system, binding of mannose to lectin leads to cleaveage of C2 and C4, which then form a C3 convertase to promote complement activation (Ricklin et al., 2010).

Suppressed platelet degranulation in severe sera

Fifteen of 17 proteins involved in platelet degranulation were down-regulated in SARS-CoV-2 infected patients, which may be associated with observed thrombocytopenia in this patient cohort (Zheng et al., 2020). Low platelet count is also reported to be associated with severe COVID-19 and mortality (Lippi et al., 2020). Two of the most intriguing proteins down-regulated in severe patients are platlet expressing chemokines pro-platelet basic protein (PPBP; also called macrophage-derived growth factor) and platelet factor 4 (PF4). PF-4 was identified as a broad-spectrum HIV-1 inhibitor at the level of virus attachment and entry via interaction with the major viral envelope glycoprotein gp120 (Auerbach et al., 2012). In another sera proteomic investigation of SARS, they found decreasing PF4 was associated with poor prognosis (Poon et al., 2012), in consistent with our findings regarding COVID-19.

Most enterochromaffin cell-derived serotonins (5-hydroxytryptamine [5-HT]) are transported to platelets for storage and release (Baganz and Blakely, 2013). Our previous data showed that when platelet counts in COVID-19 patients decrease as the severity of the disease increase (Zheng et al., 2020), serotonin (Figure 4B) level decreases accordingly. Compared with the healthy group, serotonin in non-severe and severe COVID-19 patients decreased by 2.07-fold ($p = 1.86e-04$) and 3.31-fold ($p = 9.07e-07$), respectively.

We also detected low levels of fatty acids such as arachidonate and docosapentaenoate in COVID-19 patients (Figure 4), which may be related to their decreased platelet counts. Fatty acids including arachidonate (20:4n6) are active factors of platelet degranulation. A study on H7N9 reported that H7N9 infection led to suppression of various fatty acids including palmitic acid (Sun et al., 2018). We also found palmitic acid decreased in severe COVID-19 patients.

Massive suppression of amino acids in the sera of COVID-19 patients

More than 100 decreased metabolites in the sera of COVID-19 patients are amino acids and their derivatives were found significantly decreased in the sera of COVID-19 patients compared to their levels in the healthy controls, while their levels were either unchanged or even increased in the sera of non-COVID-19 patients. Enriched in these metabolites are ten metabolites involved in arginine metabolism including glutamate, arginine, N-(l-arginino)succinate, citrulline, ornithine, glutamine, 2-oxoglutarate, N-acetyl-L-glutamate, urea, and fumarate. In addition, some arginine derivatives such as argininate, asymmetric dimethylarginine, symmetric dimethylarginine,

homoarginine and N-acetylarginine, were also significantly decreased in the sera of non-severe COVID-19 patients. It has been reported that arginine metabolism is suppressed in severe fever with thrombocytopenia syndrome caused by a SFTS bunyavirus (SFTSV)(Li et al., 2018b). Decreased arginine levels in SFTSV patients was associated with impaired anti-SFTSV functions of T cells.

DISCUSSION

Prediction of severe COVID-19 patients

Although COVID-19 can be diagnosed effectively by nucleic acid-based methods at an early stage, it is equally critical to identify severe COVID-19 patients before their manifestion of severe symptoms to minimize mortality. In this study we show that severe cases can be predicted by molecular signatures of metabolites and proteins using a machine learning model based on the expression levels of 22 serum proteins and seven metabolites (Figure 2A-B). We achieved an overall accuracy of 93.5% in the training set. Prediction of two patients did not match clinical diagnosis. One of them is non-severe individual who was the oldest patient in the training cohort. Remarkably, nine severe patients were correctly identified retrospectively based on the analysis of their sera collected one to six days before they were clinically diagnosed as having deteriorated to a severe state (Figure 1, Figure 2D), suggesting that their sera protein and metabolite signatures at the sampling time were already pointing to further deterioration into severe state even when severe clinical symptoms have not started to appear yet.

The proteins and metabolites used in our classifier (Figure 2A) contain several known biomarkers for viral infections, such as SAA2, SSA1 and CRP, which have already been used empirically to monitor the severity of COVID-19. Our study suggests that more characteristic molecular changes at protein and metabolite levels can be used to build a predictive model for the prospective identification of severe cases. The classifier also included exceptionally high levels of other acute phase proteins, including SERPINA3, among others (Figure 2A-B). Our data suggest potential benefits of broader testing of these proteins in newly diagnosed cases to identify which COVID-19 patients are likely to progress to severe disease. The model contains molecules involved in hepatic damage. The elevation of glucose, glucuronate, bilirubin degradation product and four bile acid derivatives, suggests suppressed hepatic detoxification (Rowland et al., 2013). Vascular cell adhesion protein 1 (VCAM-1) which helps to regulate transendothelial migration of leukocytes by stimulating production of reactive oxygen species (ROS), was upregulated in our data. As apotent antioxidant and inhibitor of VCAM-1 dependent cellular events (Keshavan et al., 2005), bilirubin was found to be down-regulated in our metabolomic data.

Seven patients were correctly classified in the independent validation cohort containing ten patients. Two of them could be explained by the patients' complex comorbidity and medication history. The relatively small sample size necessitates future validation studies in independent cohorts.

Molecular insights for pathogenesis of SARS-CoV-2 infection

Our data shed light on the molecular changes reflected in COVID-19 sera which could potentially yield critical diagnostic markers or therapeutic targets for managing severe COVID-19 patients (Figure 5). These molecular derangements may originate from binding of SARS-CoV-2 to alveolar macrophages via the ACE2 receptor (Hoffmann et al., 2020), resulting in release of IL-6 and TNF-α (Mehta et al., 2020) by macrophages (Gabay and Kushner, 1999). In response to elevated cytokines, especially IL-6 which triggers fever, the liver releases various APPs. Activation of APPs is accompanied with the immunogenesis or organic damage (Gabay and Kushner, 1999). Our metabolomics data also provide plausible evidence for hepatic injury. In physiological condition, hormone or bilirubin binds to glucuronate, a derivative of glucose, for liver detoxification (Rowland et al., 2013). The elevation of glucose, glucuronate, bilirubin degradation product and four bile acid derivatives in severe patients, indicating the potential declined detoxification function (Figures 4-5). Indeed, our data showed an upregulation of multiple APPs, including CRP and major attack complexes (MACs) in the severe sera. CRP can activate the complement system (Chirco and Potempa, 2018). This on the one hand leads to enhanced cytokine and chemokine production, potentially contributing to “cytokine storm"; and on the other overly recruits macrophages from the peripheral blood, which could result in acute lung injury(Chirco and Potempa, 2018; Narasaraju et al., 2011). Because about 50% of platelets are produced in the lung (Lefrancais et al., 2017), platelet may in turn respond to lung injury and activate macrophases by degranulation (Mantovani and Garlanda, 2013), which may further add to “cytokine storm”. A recent necropsy report revealed alveolar macrophage infiltration and activation in severe COVID-19 patients (Liao M., 2020), supporting our findings.

Insights for COVID-19 therapeutics

To date, few other therapies are proven effective for severe COVID-19 patients. Most of patients receive standard supportive care and antiviral therapy (Wang et al., 2020a). Corticosteroid treatment which are effectively in suppressing MERS-CoV and SARS-CoV (Arabi et al., 2018), but showed negligible effect on COVID-19 patients and may even have induced lung injury (Russell et al., 2020). The molecular changes revealed in this study in the COVID-19 sera have allowed us to propose potential new therapeutic strategies for the severe patients.

Our proteomic data showed that proteins related to platelet degranulation were substantially down-regulated in severe patients, a finding which was confirmed by low platelet counts (Zheng et al., 2020). The association between thrombocytopenia and viral infection has been observed in SARS-CoV (Zou et al., 2004), hepatitis C virus (HCV) (Assinger, 2014), and Dengue virus (Wilder-Smith et al., 2004). We thus recommend watching closely monitoring changes in platelets and making interventions, such as infusions of thrombopoietin (TPO) as necessary, particularly when liver or kidney injuries occur.

Complement activation suppresses virus invasion, and may lead to inflammatory syndromes (Barnum, 2016). Our data showed a general up-regulation of complement system proteins, including MAC proteins such as C5, C6 and C8. Suppression of complement system has been reported as an effective immunotherapeutics in SARS-infected mouse model (Gralinski et al., 2018). C5a has been reported as highly expressed in severe SARS and MERS patients as well (Wang et al., 2015). Inhibition of C5a has been reported to alleviate viral infection-induced acute lung injury (Garcia et al., 2013; Jiang et al., 2018; Sun et al., 2014). Our data suggest that severe COVID-19 patients might benefit from suppression of complement system.

The coronavirus are enveloped, positive strand RNA viruses, the replication and assembly of which consume large amount of lipids. Our metabolomics results showed that more than 100 lipids including glycerophospholipid, sphingolipids and fatty acids were down-regulated in COVID-19 patients sera, probably due to rapid replication of the virus. Glycerophospholipid, sphingolipids (one of the components of lipid rafts) and fatty acids have been reported to play an important role in the early development of enveloped viruses (Schoggins and Randall, 2013). Suppression of cholesterol synthesis by MβCD has been reported inhibiting the production of SARS-CoV particles released from infected Vero E6 cells (Li et al., 2007). Drugs inhibiting lipid synthesis such as statin have been proposed to treat HCV (Heaton and Randall, 2011) and COVID-19 (Fedson et al., 2020). Our data also supports this potential therapeutics for severe COVID-19 patients.

SARS-CoV-2 is highly infectious, applying huge pressure to the medical system worldwide. Upon COVID-19 outbreak, limited information of this pathogen was available, which restricted the collection of clinical specimens for this study. The reason for the small sample size of this study were biosafety constraints.

In conclusion, this study presents a systematic proteomic and metabolimic investigation of sera from multiple COVID-19 patient groups and control groups. We show that feasibility of predicting severe COVID-19 patients based on a panel of serum proteins and metabolites. Our data offer a landscape of blood molecular changes induced by SARS-CoV-2 infection, which may provide useful diagnositic markers and therapeutic targets.

ACKNOWLEDGEMENTS

This work is supported by grants from Westlake Special Program for COVID-19 (2020), and Tencent foundation (2020), National Natural Science Foundation of China (81972492, 21904107, 81672086), Zhejiang Provincial Natural Science Foundation for Distinguished Young Scholars (LR19C050001), Hangzhou Agriculture and Society Advancement Program (20190101A04). We thank Drs. R. Aeberold, O.L. Kon, H. Yu, D. Li, and the Guomics team for invaluable comments to this study. We thank Westlake University Supercomputer Center for assistance in data storage and computation.

AUTHOR CONTRIBUTIONS

T.G., H.C., H.L., B.S. and Y.Z. designed and supervised the project. B.S., X.B., J.D., Y.Z., J.L., J.X., Z.H., B.C., J.W., H.Y., Y.Z., D.W. and J.Z. collected the samples and clinical data. X.Y., Y.S., F.Z., R.S., L.Q., W.G., W.L., S.L., H.C., X.L., X.D., G.R., N.X., X.C., H.G., L.L., S.L., Q.X. and T.L. conducted proteomic analysis. Data were interpreted and presented by all co-authors. C.Z., S.Q., Z.K. and Z.K. conducted metabolomic analysis. T.G. wrote the manuscript with inputs from co-authors.

DECLARATION OF INTERESTS

The research group of T.G. is partly supported by Tencent, Thermo Fisher Scientific, SCIEX and Pressure Biosciences Inc. C.Z., Z.K., Z.K. and S.Q. are employees of DIAN Diagnostics.

DATA AVAILABILITY

All data are available in the manuscript or the supplementary material. The proteomics and metabolomics data are deposited in ProteomeXchange Consortium (https://www.iprox.org/). Project ID: IPX0002106000. All the data will be publicly released upon publication.

REFERENCES

Aebersold, R., and Mann, M. (2016). Mass-spectrometric exploration of proteome structure and function. Nature *537*, 347-355.

Arabi, Y.M., Mandourah, Y., Al-Hameed, F., Sindi, A.A., Almekhlafi, G.A., Hussein, M.A., Jose, J., Pinto, R., Al-Omari, A., Kharaba, A.*, et al.* (2018). Corticosteroid Therapy for Critically Ill Patients with Middle East Respiratory Syndrome. Am J Respir Crit Care Med *197*, 757-767.

Assinger, A. (2014). Platelets and infection - an emerging role of platelets in viral infection. Front Immunol *5*, 649.

Auerbach, D.J., Lin, Y., Miao, H., Cimbro, R., Difiore, M.J., Gianolini, M.E., Furci, L., Biswas, P., Fauci, A.S., and Lusso, P. (2012). Identification of the platelet-derived chemokine CXCL4/PF-4 as a broad-

spectrum HIV-1 inhibitor. Proc Natl Acad Sci U S A *109*, 9569-9574.

Baganz, N.L., and Blakely, R.D. (2013). A dialogue between the immune system and brain, spoken in the language of serotonin. ACS Chem Neurosci *4*, 48-63.

Barnum, S. (2016). Complement: A Primer for the Coming Therapeutic Revolution. Pharmacology & Therapeutics *172*.

Bindea, G., Mlecnik, B., Hackl, H., Charoentong, P., Tosolini, M., Kirilovsky, A., Fridman, W.H., Pages, F., Trajanoski, Z., and Galon, J. (2009). ClueGO: a Cytoscape plug-in to decipher functionally grouped gene ontology and pathway annotation networks. Bioinformatics *25*, 1091-1093.

Chirco, K.R., and Potempa, L.A. (2018). C-Reactive Protein As a Mediator of Complement Activation and Inflammatory Signaling in Age-Related Macular Degeneration. Frontiers in Immunology *9*, 539.

Fedson, D.S., Opal, S.M., and Rordam, O.M. (2020). Hiding in Plain Sight: an Approach to Treating Patients with Severe COVID-19 Infection. mBio *11*.

Gabay, C., and Kushner, I. (1999). Acute-Phase Proteins and Other Systemic Responses to Inflammation. New England Journal of Medicine *340*, 448-454.

Gao, H., Zhang, F., Liang, S., Zhang, Q., Lyu, M., Qian, L., Liu, W., Ge, W., Chen, C., Yi, X.*, et al.* (2020). Accelerated Lysis and Proteolytic Digestion of Biopsy-Level Fresh-Frozen and FFPE Tissue Samples Using Pressure Cycling Technology. Journal of Proteome Research.

Garcia, C.C., Weston-Davies, W., Russo, R.C., Tavares, L.P., Rachid, M.A., Alves-Filho, J.C., Machado, A.V., Ryffel, B., Nunn, M.A., and Teixeira, M.M. (2013). Complement C5 activation during influenza A infection in mice contributes to neutrophil recruitment and lung injury. PLoS One *8*, e64443-e64443.

Ghinai, I., McPherson, T.D., Hunter, J.C., Kirking, H.L., Christiansen, D., Joshi, K., Rubin, R., Morales-Estrada, S., Black, S.R., Pacilli, M.*, et al.* (2020). First known person-to-person transmission of severe acute respiratory syndrome coronavirus 2 (SARS-CoV-2) in the USA. The Lancet.

Gralinski, L.E., Sheahan, T.P., Morrison, T.E., Menachery, V.D., Jensen, K., Leist, S.R., Whitmore, A., Heise, M.T., and Baric, R.S. (2018). Complement Activation Contributes to Severe Acute Respiratory Syndrome Coronavirus Pathogenesis. mBio *9*, e01753-01718.

Gu, J.-G., Zhu, C.-l., Cheng, D.-z., Xie, Y., Liu, F., and Zhou, X. (2011). Enchanced levels of apolipoprotein M during HBV infection feedback suppresses HBV replication. Lipids Health Dis *10*, 154-154.

Guan, W.-j., Ni, Z.-y., Hu, Y., Liang, W.-h., Ou, C.-q., He, J.-x., Liu, L., Shan, H., Lei, C.-l., Hui, D.S.C.*, et al.* (2020). Clinical Characteristics of Coronavirus Disease 2019 in China. New England Journal of Medicine.

Heaton, N.S., and Randall, G. (2011). Multifaceted roles for lipids in viral infection. Trends Microbiol *19*, 368-375.

Hoffmann, M., Kleine-Weber, H., Schroeder, S., Kruger, N., Herrler, T., Erichsen, S., Schiergens, T.S., Herrler, G., Wu, N.H., Nitsche, A.*, et al.* (2020). SARS-CoV-2 Cell Entry Depends on ACE2 and TMPRSS2 and Is Blocked by a Clinically Proven Protease Inhibitor. Cell.

Hou, Y.C., Yu, H.C., Martin, R., Cirulli, E.T., Schenker-Ahmed, N.M., Hicks, M., Cohen, I.V., Jonsson, T.J., Heister, R., Napier, L.*, et al.* (2020). Precision medicine integrating whole-genome sequencing, comprehensive metabolomics, and advanced imaging. Proc Natl Acad Sci U S A *117*, 3053-3062.

Jiang, Y., Zhao, G., Song, N., Li, P., Chen, Y., Guo, Y., Li, J., Du, L., Jiang, S., Guo, R.*, et al.* (2018). Blockade of the C5a-C5aR axis alleviates lung damage in hDPP4-transgenic mice infected with

MERS-CoV. Emerg Microbes Infect *7*, 77-77.
Keshavan, P., Deem, T.L., Schwemberger, S.J., Babcock, G.F., Cook-Mills, J.M., and Zucker, S.D. (2005). Unconjugated bilirubin inhibits VCAM-1-mediated transendothelial leukocyte migration. J Immunol *174*, 3709-3718.
Kramer, A., Green, J., Pollard, J., Jr., and Tugendreich, S. (2014). Causal analysis approaches in Ingenuity Pathway Analysis. Bioinformatics *30*, 523-530.
Lee, A.H., Shannon, C.P., Amenyogbe, N., Bennike, T.B., Diray-Arce, J., Idoko, O.T., Gill, E.E., Ben-Othman, R., Pomat, W.S., van Haren, S.D.*, et al.* (2019). Dynamic molecular changes during the first week of human life follow a robust developmental trajectory. Nat Commun *10*, 1092.
Lefrancais, E., Ortiz-Munoz, G., Caudrillier, A., Mallavia, B., Liu, F., Sayah, D.M., Thornton, E.E., Headley, M.B., David, T., Coughlin, S.R.*, et al.* (2017). The lung is a site of platelet biogenesis and a reservoir for haematopoietic progenitors. Nature *544*, 105-109.
Li, G.M., Li, Y.G., Yamate, M., Li, S.M., and Ikuta, K. (2007). Lipid rafts play an important role in the early stage of severe acute respiratory syndrome-coronavirus life cycle. Microbes Infect *9*, 96-102.
Li, J., Van Vranken, J.G., Pontano Vaites, L., Schweppe, D.K., Huttlin, E.L., Etienne, C., Nandhikonda, P., Viner, R., Robitaille, A.M., Thompson, A.H.*, et al.* (2020a). TMTpro reagents: a set of isobaric labeling mass tags enables simultaneous proteome-wide measurements across 16 samples. Nat Methods.
Li, Q., Guan, X., Wu, P., Wang, X., Zhou, L., Tong, Y., Ren, R., Leung, K.S.M., Lau, E.H.Y., Wong, J.Y.*, et al.* (2020b). Early Transmission Dynamics in Wuhan, China, of Novel Coronavirus-Infected Pneumonia. N Engl J Med.
Li, T., Kim, A., Rosenbluh, J., Horn, H., Greenfeld, L., An, D., Zimmer, A., Liberzon, A., Bistline, J., Natoli, T.*, et al.* (2018a). GeNets: a unified web platform for network-based genomic analyses. Nat Methods *15*, 543-546.
Li, X.K., Lu, Q.B., Chen, W.W., Xu, W., Liu, R., Zhang, S.F., Du, J., Li, H., Yao, K., Zhai, D.*, et al.* (2018b). Arginine deficiency is involved in thrombocytopenia and immunosuppression in severe fever with thrombocytopenia syndrome. Sci Transl Med *10*.
Liang, T., Cai, H., Chen, Y., Chen, Z., Fang, Q., Han, W., Hu, S., Li, J., Li, T., Lu, X.*, et al.* (2020). Handbook of COVID-19 Prevention and Treatment
Liao M., e.a. (2020). The landscape of lung bronchoalveolar immune cells in COVID-19 revealed by single-cell RNA sequencing. medRxiv, https://doi.org/10.1101/2020.1102.1123.20026690.
Lippi, G., Plebani, M., and Henry, B.M. (2020). Thrombocytopenia is associated with severe coronavirus disease 2019 (COVID-19) infections: A meta-analysis. Clin Chim Acta *506*, 145-148.
Mantovani, A., and Garlanda, C. (2013). Platelet-macrophage partnership in innate immunity and inflammation. Nat Immunol *14*, 768-770.
Medicine, N.H.C.o.t.P.s.R.o.C.a.N.A.o.T.C. (2020). Chinese Government Diagnosis and Treatment Guideline (Trial 5th version).
Mehta, P., McAuley, D.F., Brown, M., Sanchez, E., Tattersall, R.S., Manson, J.J., and Hlh Across Speciality Collaboration, U.K. (2020). COVID-19: consider cytokine storm syndromes and immunosuppression. Lancet *395*, 1033-1034.
Minhas, P.S., Liu, L., Moon, P.K., Joshi, A.U., Dove, C., Mhatre, S., Contrepois, K., Wang, Q., Lee, B.A., Coronado, M.*, et al.* (2019). Macrophage de novo NAD(+) synthesis specifies immune function in aging and inflammation. Nat Immunol *20*, 50-63.
Murthy, S., Gomersall, C.D., and Fowler, R.A. (2020). Care for Critically Ill Patients With COVID-19.

JAMA.
Narasaraju, T., Yang, E., Samy, R.P., Ng, H.H., Poh, W.P., Liew, A.A., Phoon, M.C., van Rooijen, N., and Chow, V.T. (2011). Excessive neutrophils and neutrophil extracellular traps contribute to acute lung injury of influenza pneumonitis. Am J Pathol *179*, 199-210.
Nie, S., Zhao, X., Zhao, K., Zhang, Z., Zhang, Z., and Zhang, Z. (2020). Metabolic disturbances and inflammatory dysfunction predict severity of coronavirus disease 2019 (COVID-19): a retrospective study. medRxiv, 2020.2003.2024.20042283.
Pang, R.T., Poon, T.C., Chan, K.C., Lee, N.L., Chiu, R.W., Tong, Y.K., Chim, S.S., Sung, J.J., and Lo, Y.M. (2006). Serum amyloid A is not useful in the diagnosis of severe acute respiratory syndrome. Clin Chem *52*, 1202-1204.
Poon, T., Pang, R., Chan, K.C.A., Lee, N., Chiu, R., Tong, Y.-K., Chim, S., Ngai, S.M., Sung, J., and Lo, D. (2012). Proteomic analysis reveals platelet factor 4 and beta-thromboglobulin as prognostic markers in severe acute respiratory syndrome. Electrophoresis *33*, 1894-1900.
Ricklin, D., Hajishengallis, G., Yang, K., and Lambris, J.D. (2010). Complement: a key system for immune surveillance and homeostasis. Nat Immunol *11*, 785-797.
Rouzer, C.A., Ivanova, P.T., Byrne, M.O., Brown, H.A., and Marnett, L.J. (2007). Lipid profiling reveals glycerophospholipid remodeling in zymosan-stimulated macrophages. Biochemistry *46*, 6026-6042.
Rowland, A., Miners, J.O., and Mackenzie, P.I. (2013). The UDP-glucuronosyltransferases: Their role in drug metabolism and detoxification. The International Journal of Biochemistry & Cell Biology *45*, 1121-1132.
Russell, C.D., Millar, J.E., and Baillie, J.K. (2020). Clinical evidence does not support corticosteroid treatment for 2019-nCoV lung injury. Lancet *395*, 473-475.
Sanchez-Lopez, E., Zhong, Z., Stubelius, A., Sweeney, S.R., Booshehri, L.M., Antonucci, L., Liu-Bryan, R., Lodi, A., Terkeltaub, R., Lacal, J.C., *et al.* (2019). Choline Uptake and Metabolism Modulate Macrophage IL-1beta and IL-18 Production. Cell Metab *29*, 1350-1362 e1357.
Schoggins, J.W., and Randall, G. (2013). Lipids in innate antiviral defense. Cell Host Microbe *14*, 379-385.
Sun, S., Zhao, G., Liu, C., Fan, W., Zhou, X., Zeng, L., Guo, Y., Kou, Z., Yu, H., Li, J., *et al.* (2014). Treatment With Anti-C5a Antibody Improves the Outcome of H7N9 Virus Infection in African Green Monkeys. Clinical Infectious Diseases *60*, 586-595.
Sun, X., Song, L., Feng, S., Li, L., Yu, H., Wang, Q., Wang, X., Hou, Z., Li, X., Li, Y., *et al.* (2018). Fatty Acid Metabolism is Associated With Disease Severity After H7N9 Infection. EBioMedicine *33*, 218-229.
Team, T.N.C.P.E.R.E. (2020). The epidemiological characteristics of an outbreak of 2019 novel coronavirus diseases (COVID-19) in China. *41*, 145-151.
Thevarajan, I., Nguyen, T.H.O., Koutsakos, M., Druce, J., Caly, L., van de Sandt, C.E., Jia, X., Nicholson, S., Catton, M., Cowie, B., *et al.* (2020). Breadth of concomitant immune responses prior to patient recovery: a case report of non-severe COVID-19. Nature Medicine.
Vernon-Roberts, B. (1969). The effects of steroid hormones on macrophage activity. Int Rev Cytol *25*, 131-159.
Wang, D., Hu, B., Hu, C., Zhu, F., Liu, X., Zhang, J., Wang, B., Xiang, H., Cheng, Z., Xiong, Y., *et al.* (2020a). Clinical Characteristics of 138 Hospitalized Patients With 2019 Novel Coronavirus-Infected Pneumonia in Wuhan, China. JAMA.

Wang, R., Xiao, H., Guo, R., Li, Y., and Shen, B. (2015). The role of C5a in acute lung injury induced by highly pathogenic viral infections. Emerg Microbes Infect *4*, e28-e28.

Wang, T., Du, Z., Zhu, F., Cao, Z., An, Y., Gao, Y., and Jiang, B. (2020b). Comorbidities and multi-organ injuries in the treatment of COVID-19. Lancet *395*, e52.

Weigert, A., Weis, N., and Brune, B. (2009). Regulation of macrophage function by sphingosine-1-phosphate. Immunobiology *214*, 748-760.

Wilder-Smith, A., Earnest, A., and Paton, N.I. (2004). Use of simple laboratory features to distinguish the early stage of severe acute respiratory syndrome from dengue fever. Clin Infect Dis *39*, 1818-1823.

Wu, Z., and McGoogan, J.M. (2020). Characteristics of and Important Lessons From the Coronavirus Disease 2019 (COVID-19) Outbreak in China: Summary of a Report of 72314 Cases From the Chinese Center for Disease Control and Prevention. JAMA.

Yan, B., Chu, H., Yang, D., Sze, K.-H., Lai, P.-M., Yuan, S., Shuai, H., Wang, Y., Kao, R.Y.-T., Chan, J.F.-W*., et al.* (2019). Characterization of the Lipidomic Profile of Human Coronavirus-Infected Cells: Implications for Lipid Metabolism Remodeling upon Coronavirus Replication. Viruses *11*, 73.

Zheng, Y., Zhang, Y., Chi, H., Chen, S., Peng, M., Luo, L., Chen, L., Li, J., Shen, B., and Wang, D. (2020). The hemocyte counts as a potential biomarker for predicting disease progression in COVID-19: a retrospective study. CCLM clinical chemistry and laboratory medicine *58*.

Zhou, Y., Zhou, B., Pache, L., Chang, M., Khodabakhshi, A.H., Tanaseichuk, O., Benner, C., and Chanda, S.K. (2019). Metascape provides a biologist-oriented resource for the analysis of systems-level datasets. Nat Commun *10*, 1523.

Zou, Z., Yang, Y., Chen, J., Xin, S., Zhang, W., Zhou, X., Mao, Y., Hu, L., Liu, D., Chang, B*., et al.* (2004). Prognostic factors for severe acute respiratory syndrome: a clinical analysis of 165 cases. Clin Infect Dis *38*, 483-489.

586 **Table 1. Demographics and baseline characteristics of COVID-19 patients.**
587

Variables	Healthy Control (N=28)	non-COVID-19 (N=25)	COVID-19		
			Total (N=46)	non-Severe (N=25)	Severe (N=21)
Sex - no. [a] (%)					
Male	21 (75.0)	17 (68.0)	31 (67.4)	18 (72.0)	13 (61.9)
Female	7 (25.0)	8 (32.0)	15 (32.6)	7 (28.0)	8 (38.1)
Age - yr. [b]					
Mean ± SD	44.4±8.3	49.2±14.0	47.7±13.9	42.2±12.8	54.3±12.4
Median (IQR)	45.0 (38.0-51.0)	53.0 (37.0-61.0)	46.5 (35.8-59.0)	43.0 (33.0-50.0)	55.0 (47.0-63.0)
Range	28.0-57.0	23.0-67.0	20.0-75.0	20.0-70.0	30.0-75.0
BMI, kg/m^2					
Mean ± SD [c]	24.4±2.7	23.5±2.7	24.9±3.0	24.5±3.3	26.0±2.4
Median (IQR) [d]	24.2 (22.5-26.5)	24.7 (20.9-25.8)	24.8 (22.7-27.0)	24.9 (21.7-26.8)	25.8 (24.4-28.0)
Range	19.9-32.9	19.1-27.4	19.0-31.3	18.9-30.4	22.2-31.3
Smoke - no. (%)			5 (10.9)	2 (8.0)	1 (4.8)
Alcohol - no. (%)			1 (2.2)	1 (4.0)	0 (0.0)
Time from onset to admission, days					
Mean ± SD			3.0±4.2	1.6±2.1	4.6±5.4
Median (IQR)			1.5 (0.0-4.0)	1.0 (0.0-2.0)	2.0 (0.5-6.0)
Range			0.0-20.0	0.0-10.0	0.0-20.0
Time from admission to severe, days					
Mean ± SD					4.0±2.1
Median (IQR)					4.0 (2.5-5.5)
Range					0.0-7.0
Symptoms - no. (%)					
Fever		9 (36.0)	34 (73.9)	16 (64.0)	18 (85.7)
Cough		11 (44.0)	26 (56.5)	13 (52.0)	13 (61.9)
Headache		2 (8.0)	7 (15.2)	4 (16.0)	3 (14.3)
Fatigue		2 (8.0)	8 (17.4)	5 (20.0)	3 (14.3)
Pharyngalgia		0 (0.0)	3 (6.5)	1 (4.0)	2 (9.5)
Expectoration		3 (12.0)	12 (26.1)	4 (16.0)	8 (38.1)
Diarrhea		0 (0.0)	3 (6.5)	1 (4.0)	2 (9.5)
Chest tightness		2 (8.0)	1 (2.2)	1 (4.0)	0 (0.0)
Chest CT [e] - no. (%)					
Involvement of chest radiographs		1 (4.0)	45 (97.8)	24 (96.0)	21 (100)
Comorbidity- no. (%)					
Hypertension		10 (40.0)	6 (13.0)	1 (4.0)	5 (23.8)
Diabetes		0 (0.0)	6 (13.0)	3 (12.0)	3 (14.3)

Respiratory system	2 (8.0)	4 (8.7)	3 (12.0)	1 (4.8)
Endocrine system	0 (0.0)	3 (6.5)	0 (0.0)	3 (14.3)
Chronic kidney disease	0 (0.0)	1 (2.2)	0 (0.0)	1 (4.8)
Digestive system	2 (8.0)	6 (13.0)	3 (12.0)	3 (14.3)
Oxygenation Index - mmHg				
Mean ± SD			478.4±147.5	347.4±124.1
Median (IQR)			447.6 (390.5-506.0)	341.4 (266.5-381.9)
Range			289.7-890.5	133.3-728.6
Treatment - no. (%)				
Oxygen inhalation	3 (12.0)	30 (65.2)	10 (40.0)	20 (95.2)
Antibiotics	0 (0.0)	15 (32.6)	8 (32.0)	7 (33.3)
Antiviral drug	25 (100)	46 (100.0)	25 (100.0)	21 (100.0)
Immunoglobulin	0 (0.0)	19 (41.3)	0 (0.0)	19 (90.5)
Methylprednisolone	0 (0.0)	16 (34.8)	0 (0.0)	16 (76.2)
Chinese medicine	0 (0.0)	45 (97.8)	25 (100.0)	20 (95.2)

[a] no. (%): number.

[b] yr.: year.

[c] SD: Standard Deviation.

[d] IQR: Interquartile range

[e] CT: Computed tomography

Figure 1. Summary of COVID-19 patients and machine learning design. (A) Summary of COVID-19 patients, including non-severe (n=25) and severe (n=21) patients with more details in Table S1. Patients labeled in red (Y-axis) indicate chronic infection of viruses including HBV. (B) Study design for machine learning-based classifier development for severe COVID-19 patients. We first procured samples in a training cohort for proteomic and metabolomic analysis. The classifier was then validated in an independent cohort.

Figure 2. Separation of severe and non-severe COVID-19 patients by machine learning of proteomic and metabolomic features. (A) Top 22 proteins and 7 metabolites prioritized by random forest analysis ranked by the mean decrease in accuracy. (B) Network of prioritized proteins appeared in the classifier. (C) ROC of the random forest model in the training cohort. (D) Principal Components Analysis (PCA) plot of COVID-19 patients from the training cohort. (E) Performance of the model in the validation cohort of ten COVID-19 patients. Patients labeled in red received serum test before they were diagnosed as severe.

Figure 3. Dysregulated proteins in COVID-19 sera. (A) Heatmap of 50 selected proteins whose regulation concentrated on three enriched pathways. (B) The expression level change (z-scored original value) of six selected proteins of interest with significance indicated by the asterisks (unpaired two sided Welch's t test. p value: ***, <0.001; **, <0.01; *, <0.05)

Figure 4. Dysregulated metabolites in COVID-19 sera. (A) Heatmap of 82 regulated metabolites belonging to six major classes: fatty acids, steroids, glycerophospholipid, sphingolipid, choline and serotonins. (B) The expression level change (z-scored log2 original value) of six regulated metabolites from each metabolite class with significance indicated by the asterisks as described in Figure 3.

Figure 5. Key proteins and metabolites characterized in severe COVID-19 patients in a working model. SARS-CoV-2 may target alveolar macrophages via ACE2 receptor with increasing level of cytokines including IL-6 and TNF-α, which subsequently induce the elevation of various APPs such as SAP, CRP, SAA1, SAA2 and C6 which are significantly upregulated in the severe group. Proteins involved in macrophage, lipid metabolism and platelet degranulation were indicated with their corresponding expression levels in four patient groups.

MATERIALS AND METHODS

Patients and samples

Our team procured serum samples from 46 patients who visited Taizhou Public Health Medical Center during January 23 and February 4, 2020. They were diagnosed as COVID-19 according to the Chinese Government Diagnosis and Treatment Guideline (Trial 5th version)(Medicine, 2020). For diagnosing COVID-19, nucleic acid from sputum or throat swab was extracted using nucleic acid extractor (Shanghai Zhijiang, China, EX3600) and virus nucleic acid extraction reagent (Shanghai Zhijiang, China, NO. P20200201) was used to extract nucleic acid. Fluorescence quantitative PCR (ABI7500) and SARS-CoV-2 nucleic acid detection kit (triple fluorescence PCR, Shanghai Zhijiang, China, NO. P20200203) were used for nucleic acid detection. This kit uses one step RT-PCR combined with Taqman technology to detect RdRp, E and N genes. Positive was concluded if RdRp gene was positive (Ct < 43), and one of E or N was positive (Ct <43). Patients were also diagnosed as positive if two sequential tests of RdRp were positive while E and N were negative. According to the abovementioned guideline, COVID-19 patients are classified into four subgroups: 1) Mild: mild symptoms without pneumonia; 2) Typical: fever or respiratory tract symptoms with pneumonia; 3) Severe: fulfill any of the three criteria: respiratory distress, respiratory rate ≥ 30 times/min; means oxygen saturation ≤ 93% in resting state; arterial blood oxygen partial pressure/oxygen concentration ≤ 300 mmHg (1 mmHg = 0.133 kPa); 4) Critical: fulfill any of the three criteria: respiratory failure and require mechanical ventilation; shock incidence; admission to ICU with other organ failure. In this study, we included both severe and no-severe patients, with the latter composed of mild and typical COVID-19 patients. Last follow-up of these patients was March 10, 2020. We also procured 25 non-COVID-19 patients with similar clinical characteristics including fever and/or cough as COVID-19 patients however negative in the nucleic acid test. Based on the Chinese Government Diagnosis and Treatment Guideline (Trial 5th version) (Medicine, 2020), patients are defined as suspected COVID-19 cases when they meet the following three clinical criteria: 1) fever or respiratory symptoms, 2) imaging manifestation of pneumonia, and 3) optional reduction of white blood cell or lymphocyte count at early stage. The patients only need to meet at least two of the above three criteria if they have been exposed to COVID-19 individuals. We also collected serum samples from 28 healthy individuals as control. All the serum samples were collected as venous whole blood in the early morning before diet using serum separation tubes (Zhejiang GongDong Medical Technology Co., Ltd, China). The blood samples were centrifuged at 3,500 rpm for 10 min for serum collection. The serum samples were frozen at -80℃. The samples from this study is from a clinical trial that our team initiated and registered in the Chinese Clinical Trial Registry with a ID of ChiCTR2000031365. This study has been approved by the

Ethical/Institutional Review Board of Taizhou Public Health Medical Center and Westlake University. Contents from patients were waived by the boards.

Proteomic analysis

Serum samples were inactivated and sterilized at 56℃ for 30 min, and processed as previously with some modifications. Five μL serum from each specimen was lysed in 50 μL lysis buffer (8 M urea in 100 mM triethylammonium bicarbonate, TEAB) at 32℃ for 30 min. The lysates were reductive with 10 mM tris (2-carboxyethyl) phosphine (TCEP) for 30 min at 32℃, then alkylated for 45 min with 40 mM iodoacetamide (IAA) in darkness at room temperature (25℃). The protein extracts were diluted with 200 μL 100 mM TEAB, and digested with double-step trypsinization (Hualishi Tech. Ltd, Beijing, China), each step with an enzyme-to-substrate ratio of 1:20, at 32℃ for 60 min. The reaction was stopped by adding 30 μL 10% trifluoroacetic acid (TFA) in volume. Digested peptides were cleaned-up with SOLAμ (Thermo Fisher Scientific™, San Jose, USA) following the manufacturer's instructions, and lableled with TMTpro 16plex label reagents (Thermo Fisher Scientific™, San Jose, USA) as described previously. The TMT samples were fractionated using a nanoflow DIONEX UltiMate 3000 RSLCnano System (Thermo Fisher Scientific™, San Jose, USA) with an XBridge Peptide BEH C18 column (300 Å, 5 μm × 4.6 mm × 250 mm) (Waters, Milford, MA, USA)(Gao et al., 2020). The samples were separated using a gradient from 5% to 35% acetonitrile (ACN) in 10 mM ammonia (pH=10.0) at a flow rate of 1 mL/min. Peptides were separated into 120 fractions, which were consolidated into 40 fractions. The fractions were subsequently dried and re-dissolved in 2% ACN/0.1% formic acid (FA). The re-dissolved peptides were analyzed by LC-MS/MS with the same LC system coupled to a Q Exactive HF-X hybrid Quadrupole-Orbitrap (Thermo Fisher Scientific™, San Jose, USA) in data dependent acquisition (DDA) mode. For each acquisition, peptides were loaded onto a precolumn (3 μm, 100 Å, 20 mm*75 μm i.d.) at a flowrate of 6 μL/min for 4 min and then injected using a 35 min LC gradient (from 5% to 28% buffer B) at a flowrate of 300 nL/min (analytical column, 1.9 μm, 120 Å, 150 mm*75 μm i.d.). Buffer A was 2%ACN, 98% H_2O containing 0.1% FA, and buffer B was 98% ACN, 2% H_2O containing 0.1% FA. All reagents were MS grade. The *m/z* range of MS1 was 350-1,800 with the resolution at 60,000 (at 200 *m/z*), AGC target of 3e6, and maximum ion injection time (max IT) of 50 ms. Top 15 precursors were selected for MS/MS experiment, with a resolution at 45,000 (at 200 *m/z*), AGC target of 2e5, and max IT of 120 ms. The isolation window of selected precursor was 0.7 *m/z*. The resultant mass spectrometric data were analyzed using Proteome Discoverer (Version 2.4.1.15, Thermo Fisher Scientific) using a protein database composed of the *Homo sapiens* fasta database downloaded from UniprotKB on 07 Jan 2020 and the SARS-CoV-2 virus fasta downloaded from NCBI (version NC_045512.2). Enzyme was set to trypsin with two missed cleavage tolerance. Static modifications were set to

carbamidomethylation (+57.021464) of cysteine, TMTpro (+304.207145) of lysine residues and peptides' N termini, and variable modifications were set to oxidation (+15.994915) of methionine and acetylation (+42.010565) of peptides' N-termini. Precursor ion mass tolerance was set to 20 ppm, and product ion mass tolerance was set to 0.06 Da. The peptide-spectrum-match allowed 1% target false discovery rate (FDR) (strict) and 5% target FDR (relaxed). Normalization was performed against the total peptide amount. The other parameters followed the default setup.

Quality control of proteomic data

The quality of proteomic data was ensured at multiple levels. First, a mouse liver digest was used for instrument performance evaluation. We also run water samples (buffer A) as blanks every 4 injections to avoid carry-over. Serum samples of four patient groups from both training and validation cohorts were randomly distributed in eight different batches. Six samples were injected in technical replicates.

Metabolomic analysis

Ethanol was added to the serum samples and shaken vigorously to inactivate any potential viruses, then dried in a biosafety hood. The dried samples were further treated for metabolomics analysis. The metabolomic analysis was performed as described previously(Lee et al., 2019). Briefly, deactivated serum samples, 100 µL each, were extracted by adding 300 µL extraction solution. The mixtures were shaken vigorously for 2 min. Proteins were denatured and precipitated by centrifugation. The supernatants contained metabolites of diverse chemical natures. To ensure the quantity and reliability of metabolite detection, four platforms were performed with non-target metabolomics. Each supernatant was divided into four fractions: two for analysis using two separate reverse-phase /ultra-performance liquid chromatography (RP/UPLC)-MS/MS methods with positive ion-mode electrospray ionization (ESI), one for analysis using RP/ UPLC-MS/MS with negative-ion mode ESI, and one for analysis using hydrophilic interaction liquid chromatography (HILIC)/UPLC-MS/MS with negative-ion mode ESI. Each fraction was dried under nitrogen gas to remove the organic solvent and later re-dissolved in four different reconstitution solvents compatible with each of the four UPLC-MS/MS methods.

All UPLC-MS/MS methods used ACQUITY 2D UPLC system (Waters, Milford, MA, USA) and Q Exactive HF hybrid Quadrupole-Orbitrap (Thermo Fisher Scientific™, San Jose, USA) with HESI-II heated ESI source and Orbitrap mass analyzer. The mass spectrometer was operated at 35,000 mass resolution (at 200 *m/z*). In the first UPLC-MS/MS method, the QE was operated under positive electron spray ionization (ESI) coupled with a C18 column (UPLC BEH C18, 2.1 × 100 mm, 1.7 µm; Waters) was used in UPLC. The mobile solutions used in the gradient elution were water and methanol

containing 0.05% perfluoropentanoic acid (PFPA) and 0.1% FA. In the second method, the QE was still operated under ESI positive mode, and the UPLC used the same C18 column as in method one, but the mobile phase solutions were optimized for more hydrophobic compounds and contained methanol, acetonitrile, water, 0.05% PFPA, and 0.01% FA. The third method had the QE operated under negative ESI mode, and the UPLC method used a C18 column eluted with mobile solutions containing methanol and water in 6.5 mM ammonium bicarbonate at pH 8. The UPLC column used in the fourth method was HILIC column (UPLC BEH Amide, 2.1 × 150 mm, 1.7 μm; Waters), and the mobile solutions were consisted of water and acetonitrile with 10 mM ammonium formate at pH 10.8; the QE was operated under negative ESI mode. The QE mass spectrometer analysis was alternated between MS and data-dependent MS2 scans using dynamic exclusion. The scan range was 70-1,000 *m/z*.

After raw data pre-processing, peak finding/alignment, and peak annotation using in-house software, metabolites were identified by searching an in-house library containing more than 3,300 standards with library data entries generated from running purified compound standards through the experimental platforms. Identification of metabolites must meet three strict criteria: narrow window retention index (RI), accurate mass with variation less than 10 ppm and MS/MS spectra with high forward and reverse scores based on comparisons of the ions present in the experimental spectrum to the ions present in the library spectrum entries. Almost all isomers can be distinguished by these three criteria. All identified metabolites meet the level 1 requirements by the Chemical Analysis Working Group (CAWG) of the Metabolomics Standards Initiative (MSI) expect some asterisk labeled lipids which MS/MS spectral were *in silico* matched.

Quality control of metabolomics analysis

Several types of quality control samples were included in the experiment: a pooled sample generated by taking a small volume of each experimental sample to serve as a technical replicate that was run multiple times throughout the experiment, extracted water samples served as blanks, and extracted commercial plasma samples for monitoring instrument variation. A mixture of internal standards was also spiked into every sample to aid chromatographic peak alignment and instrument stability monitoring. Instrument variability was determined by calculating the median relative SD (RSD) of all internal standards in each sample. The experimental process variability was determined by calculating the median RSD for all endogenous metabolites present in the pooled quality control samples.

Statistical analysis

Metabolites and therapeutic compounds with over 80% missing ratios in a particular patient group were removed for the metabolomics dataset

containing endogenoeous metabolites while full proteomics features were used for the subsequent statistical analysis. Missing values were imputated with the minimal value for each feature. Log2 fold-change (log2 FC) was calculated on the mean of the same patient group for each pair of comparing groups. Two-sided unpaired Welch's t test was performed for each pair of comparing groups and adjusted p values were calculated using Benjamini & Hochberg correction. The statistical significantly changed proteins or metabolites were selected using the criteria of adjust p value less than 0.05 indicated and absolute log2 FC larger than 0.25. From the training cohort, the important features were selected with mean decrease accuracy larger than 3 using random forest containing a thousand trees using R package randomForest (version 4.6.14) random forest analysis with 10-fold cross validation as binary classification of paired severe and non-severe group using combined differentially regulated proteins and metabolites features. The random forest analysis was further performed for a hundred times on the matrix with only the selected important features using normalized additive predicting probability as the final predicting probability and the larger probability as the predictive label. Those selected important features were used for the random forest analysis on the independent validation cohort.

Pathway analysis

Four network pathway analysis tools were used for pathway analysis using 93 differentially expressed proteins (DEPs). The top Gene Ontology (GO) processes were enriched by Metascape web-based platform (Zhou et al., 2019). The GO terms is enriched using the Cytoscape plug-in ClueGO (Bindea et al., 2009). Ingenuine pathway analysis (Kramer et al., 2014) of the regulated proteins identifies most significantly relevant pathways with p value of determined based on right-tailed Fisher's Exact Test with the overall activation or inhibition states of enriched pathways were predicted by z-score. Functional co-expression network analysis by GeNet(Li et al., 2018a) to represent statistical co-expressed protein modules.

Figure S1. Quality control of proteomic and metabolomic data. (A) Coefficient of variation (CV) of the proteomic data is calculated by the proteins quantified in six quality control (QC) samples using the pooled samples from all samples in training cohort. CV of the metabolomic data is calculated by twelve QC samples using a set of isotopic internal spiked-in standards. (B) UMAP of sera samples using 791 measured proteins. (C) UMAP of sera samples using 847 metabolites.

Figure S2. Differentially expressed proteins in different patient groups in the training cohort. Volcano plots compare four pairs of patient groups as indicated in the plot. Proteins with log2 (fold-change) beyond 0.25 or below -0.25 with adjusted p value lower than 0.05 were considered as significantly differential expression. Number of significantly down- (blue) and up- (red) regulated proteins were shown on the top.

Figure S3. Differentially expressed metabolites in different patient groups in the training cohort. The volcano plots follow that for Figure S3 except metabolomic data were used as the input.

Figure S4. Proteins and metabolites regulated in COVID-19 patients but not in non-COVID-19 patients. Venn diagrams showing the overlaps between significantly regulated proteins (A) and metabolites (B) as identified in volcano plots. Proteins and metabolites labeled in red are the shortlisted molecules which differentially expressed in the COVID-19 patients but not in the non-COVID-19 patients.

Figure S5. Identification of specific clusters of proteins and metabolites in COVID-19 patients. 791 proteins (A) and 941 metabolites (B) were clustered using mFuzz into 16 significant discrete clusters, respectively, to illustrate the relative expression changes of the proteomics and metabolomics data. The groups in proteomics data: 1: Healthy; 2: non-Severe COVID-19; 3: Severe COVID-19. The groups in metabolomics data: 1: Healthy; 2: non-COVID-19; 3: non-Severe COVID-19; 4: Severe COVID-19.

Figure S6. Pathway analysis of 93 differential expressed proteins in COVID-19 patients. (A) The Gene Ontology (GO) processes enriched by Metascape. (B) The GO terms enriched using the Cytoscape plug-in ClueGO. (C) Ingenuine pathway analysis of most significantly relevant pathways with the predicted activation or inhibition state. (D) Functional network analysis by GeNet identifies several communities.

Figure 1

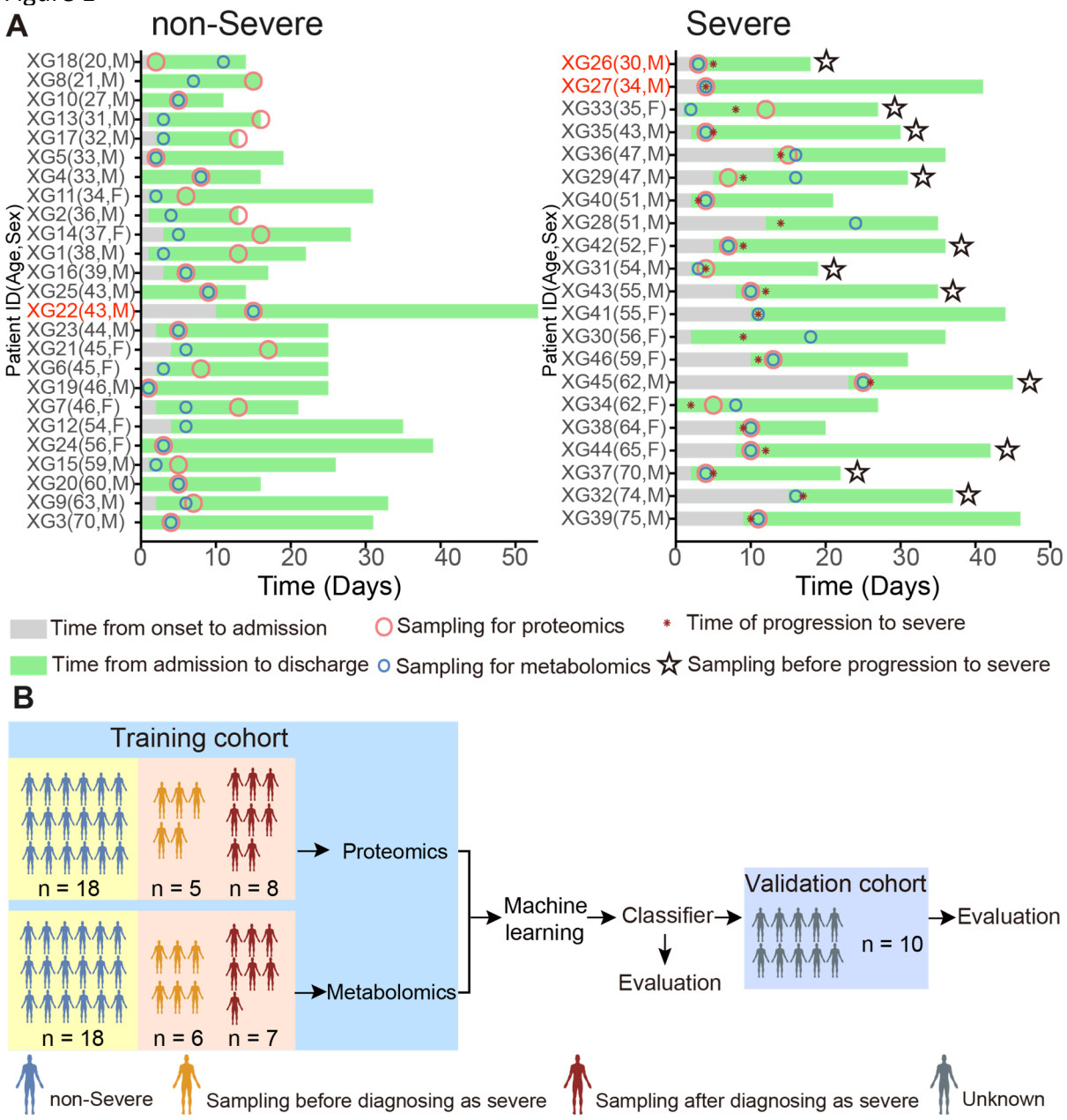
A
non-Severe
Severe
Patient ID(Age,Sex)
XG18(20,M)
XG8(21,M)
XG10(27,M)
XG13(31,M)
XG17(32,M)
XG5(33,M)
XG4(33,M)
XG11(34,F)
XG2(36,M)
XG14(37,F)
XG1(38,M)
XG16(39,M)
XG25(43,M)
XG22(43,M)
XG23(44,M)
XG21(45,F)
XG6(45,F)
XG19(46,M)
XG7(46,F)
XG12(54,F)
XG24(56,F)
XG15(59,M)
XG20(60,M)
XG9(63,M)
XG3(70,M)
XG26(30,M)
XG27(34,M)
XG33(35,F)
XG35(43,M)
XG36(47,M)
XG29(47,M)
XG40(51,M)
XG28(51,M)
XG42(52,F)
XG31(54,M)
XG43(55,M)
XG41(55,F)
XG30(56,F)
XG46(59,F)
XG45(62,M)
XG34(62,F)
XG38(64,F)
XG44(65,F)
XG37(70,M)
XG32(74,M)
XG39(75,M)
0
10
20
30
40
50
Time (Days)
Time from onset to admission
Time from admission to discharge
Sampling for proteomics
Sampling for metabolomics
Time of progression to severe
Sampling before progression to severe
B
Training cohort
n = 18
n = 5
n = 8
n = 18
n = 6
n = 7
Proteomics
Metabolomics
Machine learning
Classifier
Evaluation
Validation cohort
n = 10
Evaluation
non-Severe
Sampling before diagnosing as severe
Sampling after diagnosing as severe
Unknown

Figure 2

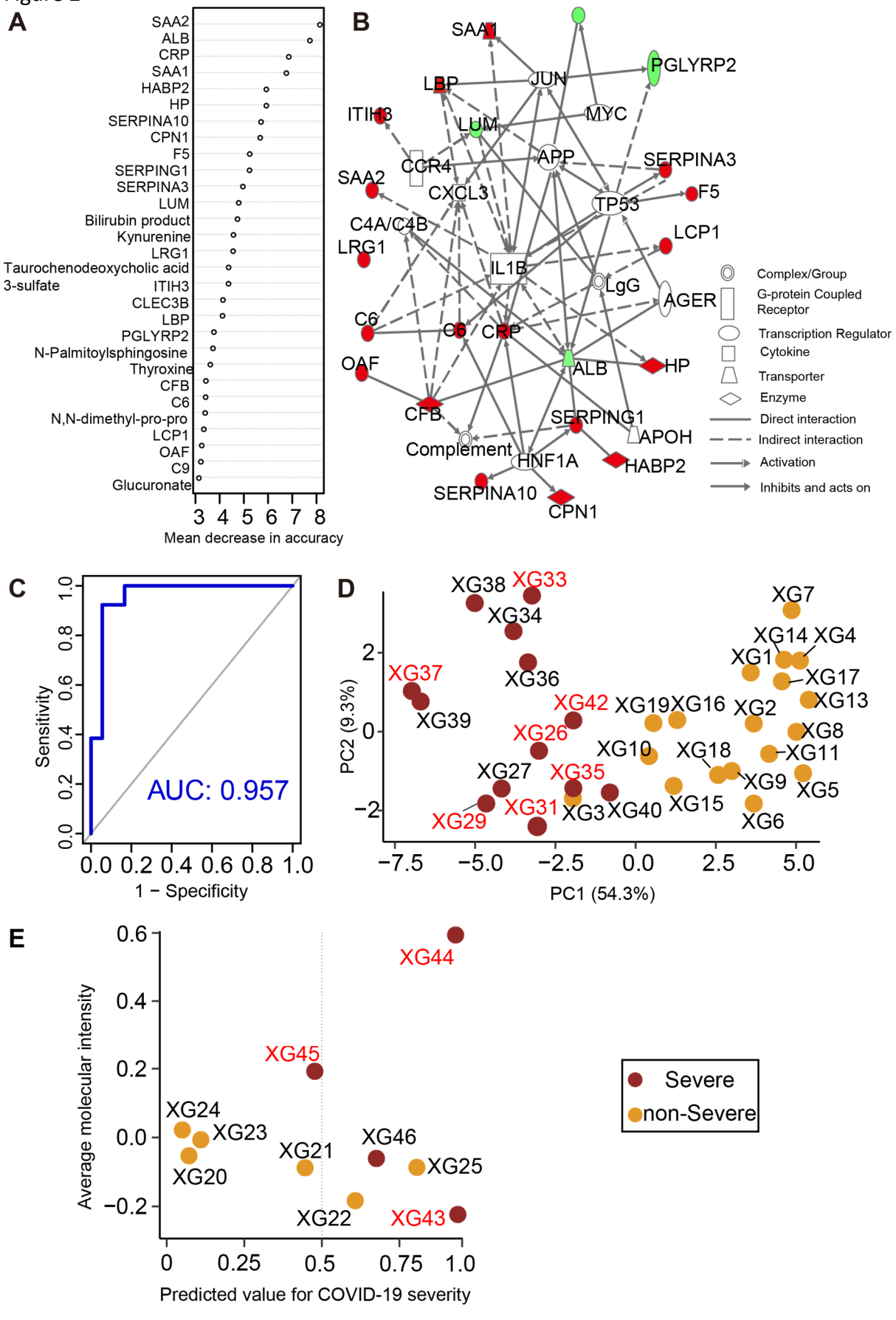
A
SAA2
ALB
CRP
SAA1
HABP2
HP
SERPINA10
CPN1
F5
SERPING1
SERPINA3
LUM
Bilirubin product
Kynurenine
LRG1
Taurochenodeoxycholic acid 3-sulfate
ITIH3
CLEC3B
LBP
PGLYRP2
N-Palmitoylsphingosine
Thyroxine
CFB
C6
N,N-dimethyl-pro-pro
LCP1
OAF
C9
Glucuronate
3 4 5 6 7 8
Mean decrease in accuracy
B
SAA1
PGLYRP2
LBP
JUN
ITIH3
LUM
MYC
APP
SERPINA3
CCR4
SAA2
CXCL3
F5
TP53
C4A/C4B
LCP1
LRG1
IL1B
LgG
AGER
C6
C6
CRP
OAF
ALB
HP
CFB
SERPING1
APOH
Complement
HNF1A
HABP2
SERPINA10
CPN1
Complex/Group
G-protein Coupled Receptor
Transcription Regulator
Cytokine
Transporter
Enzyme
Direct interaction
Indirect interaction
Activation
Inhibits and acts on
C
Sensitivity
1 − Specificity
AUC: 0.957
D
PC2 (9.3%)
PC1 (54.3%)
XG38
XG33
XG34
XG7
XG14
XG4
XG1
XG17
XG37
XG36
XG13
XG42
XG19
XG16
XG2
XG39
XG26
XG8
XG10
XG18
XG11
XG27
XG35
XG9
XG5
XG31
XG3
XG40
XG15
XG29
XG6
E
Average molecular intensity
Predicted value for COVID-19 severity
XG44
XG45
XG24
XG23
XG46
XG21
XG25
XG20
XG22
XG43
Severe
non-Severe

Figure 3

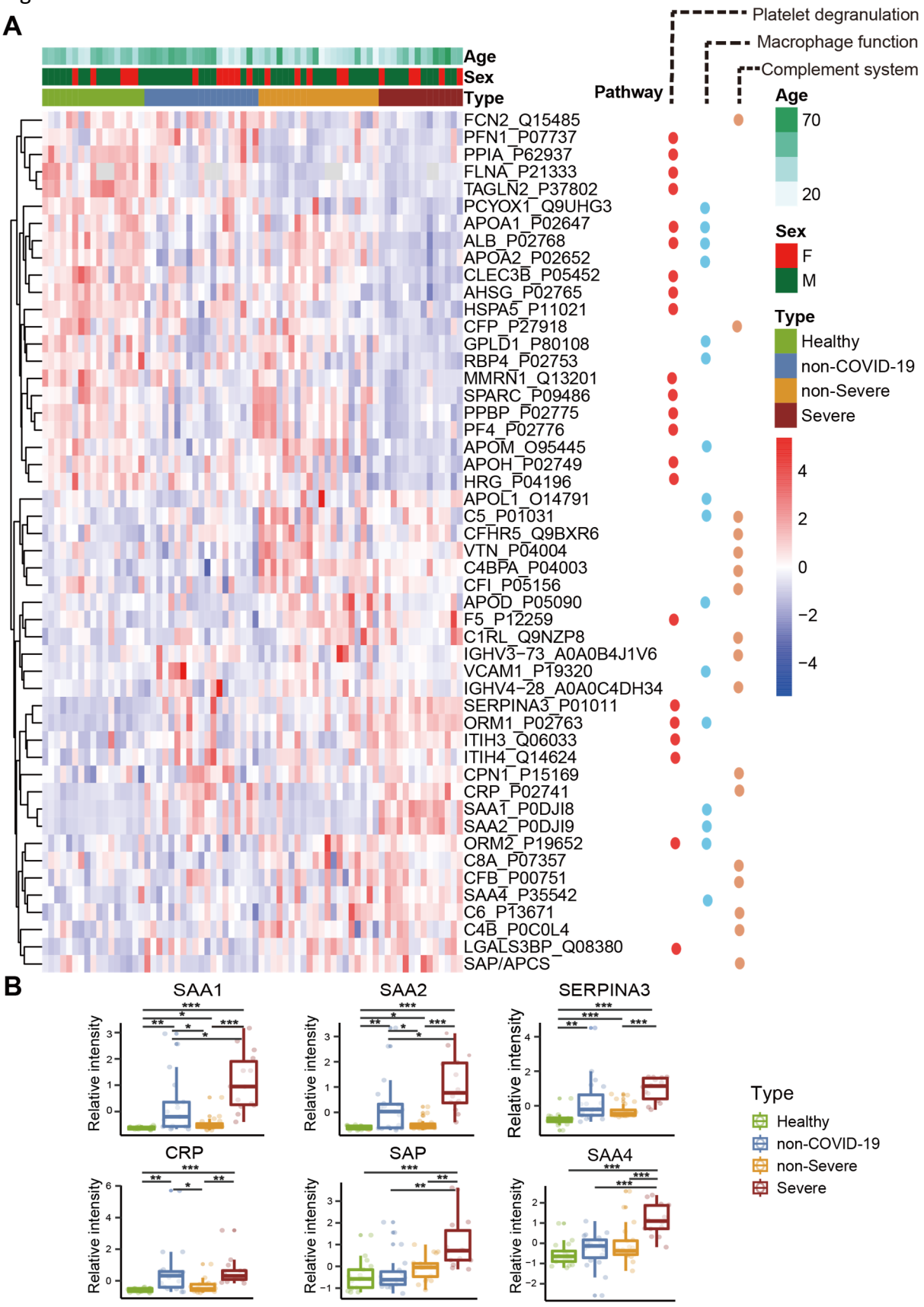
A
Age
Sex
Type
Pathway
Platelet degranulation
Macrophage function
Complement system
FCN2_Q15485
PFN1_P07737
PPIA_P62937
FLNA_P21333
TAGLN2_P37802
PCYOX1_Q9UHG3
APOA1_P02647
ALB_P02768
APOA2_P02652
CLEC3B_P05452
AHSG_P02765
HSPA5_P11021
CFP_P27918
GPLD1_P80108
RBP4_P02753
MMRN1_Q13201
SPARC_P09486
PPBP_P02775
PF4_P02776
APOM_O95445
APOH_P02749
HRG_P04196
APOL1_O14791
C5_P01031
CFHR5_Q9BXR6
VTN_P04004
C4BPA_P04003
CFI_P05156
APOD_P05090
F5_P12259
C1RL_Q9NZP8
IGHV3-73_A0A0B4J1V6
VCAM1_P19320
IGHV4-28_A0A0C4DH34
SERPINA3_P01011
ORM1_P02763
ITIH3_Q06033
ITIH4_Q14624
CPN1_P15169
CRP_P02741
SAA1_P0DJI8
SAA2_P0DJI9
ORM2_P19652
C8A_P07357
CFB_P00751
SAA4_P35542
C6_P13671
C4B_P0C0L4
LGALS3BP_Q08380
SAP/APCS
Age
70
20
Sex
F
M
Type
Healthy
non-COVID-19
non-Severe
Severe
4
2
0
−2
−4
B
SAA1
SAA2
SERPINA3
CRP
SAP
SAA4
Relative intensity
Type
Healthy
non-COVID-19
non-Severe
Severe

Figure 4

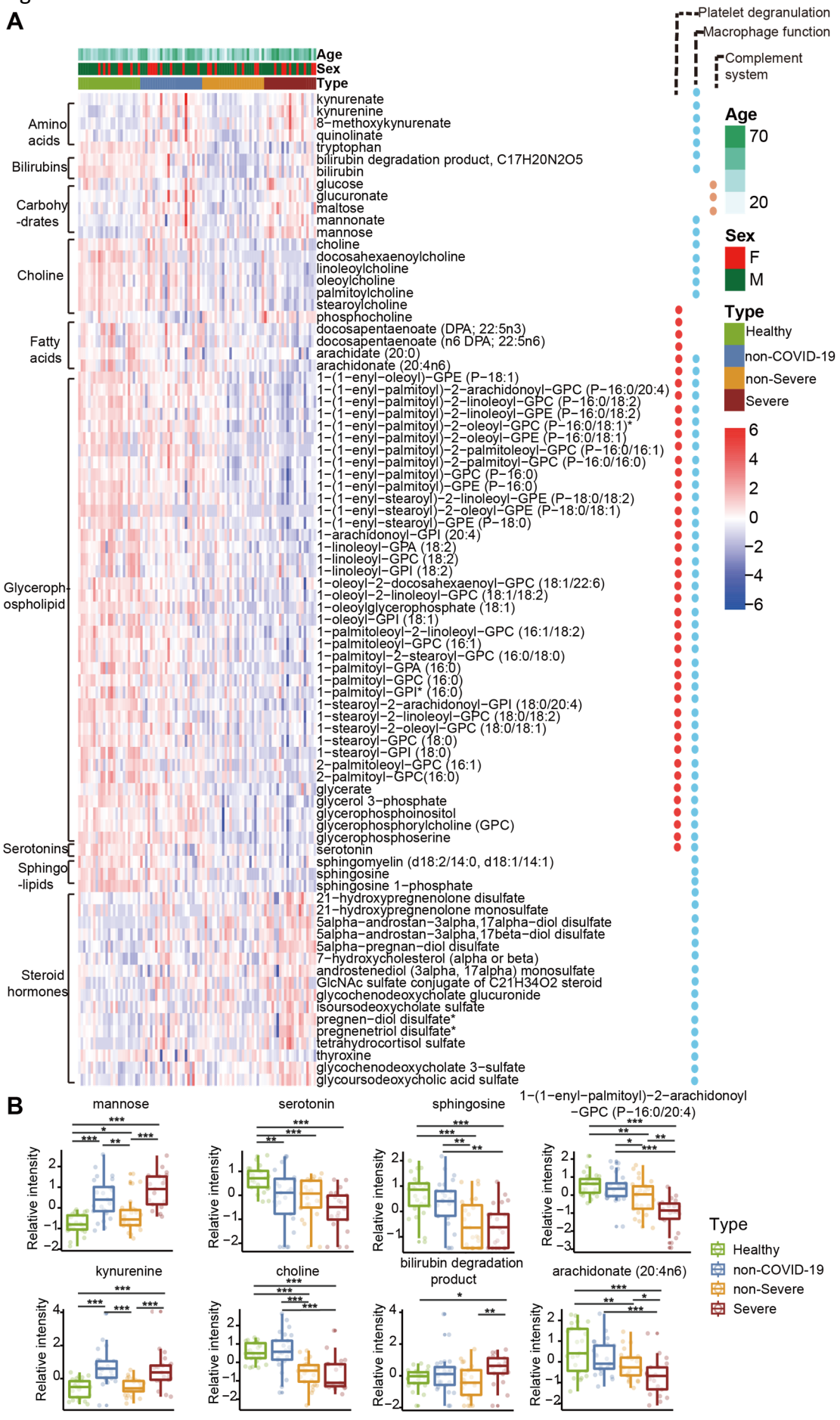
A
Platelet degranulation
Macrophage function
Complement system
Age
Sex
Type
Amino acids
Bilirubins
Carbohy-drates
Choline
Fatty acids
Glycerophospholipid
Serotonins
Sphingo-lipids
Steroid hormones
kynurenate
kynurenine
8−methoxykynurenate
quinolinate
tryptophan
bilirubin degradation product, C17H20N2O5
bilirubin
glucose
glucuronate
maltose
mannonate
mannose
choline
docosahexaenoylcholine
linoleoylcholine
oleoylcholine
palmitoylcholine
stearoylcholine
phosphocholine
docosapentaenoate (DPA; 22:5n3)
docosapentaenoate (n6 DPA; 22:5n6)
arachidate (20:0)
arachidonate (20:4n6)
1−(1−enyl−oleoyl)−GPE (P−18:1)
1−(1−enyl−palmitoyl)−2−arachidonoyl−GPC (P−16:0/20:4)
1−(1−enyl−palmitoyl)−2−linoleoyl−GPC (P−16:0/18:2)
1−(1−enyl−palmitoyl)−2−linoleoyl−GPE (P−16:0/18:2)
1−(1−enyl−palmitoyl)−2−oleoyl−GPC (P−16:0/18:1)*
1−(1−enyl−palmitoyl)−2−oleoyl−GPE (P−16:0/18:1)
1−(1−enyl−palmitoyl)−2−palmitoleoyl−GPC (P−16:0/16:1)
1−(1−enyl−palmitoyl)−2−palmitoyl−GPC (P−16:0/16:0)
1−(1−enyl−palmitoyl)−GPC (P−16:0)
1−(1−enyl−palmitoyl)−GPE (P−16:0)
1−(1−enyl−stearoyl)−2−linoleoyl−GPE (P−18:0/18:2)
1−(1−enyl−stearoyl)−2−oleoyl−GPE (P−18:0/18:1)
1−(1−enyl−stearoyl)−GPE (P−18:0)
1−arachidonoyl−GPI (20:4)
1−linoleoyl−GPA (18:2)
1−linoleoyl−GPC (18:2)
1−linoleoyl−GPI (18:2)
1−oleoyl−2−docosahexaenoyl−GPC (18:1/22:6)
1−oleoyl−2−linoleoyl−GPC (18:1/18:2)
1−oleoylglycerophosphate (18:1)
1−oleoyl−GPI (18:1)
1−palmitoleoyl−2−linoleoyl−GPC (16:1/18:2)
1−palmitoleoyl−GPC (16:1)
1−palmitoyl−2−stearoyl−GPC (16:0/18:0)
1−palmitoyl−GPA (16:0)
1−palmitoyl−GPC (16:0)
1−palmitoyl−GPI* (16:0)
1−stearoyl−2−arachidonoyl−GPI (18:0/20:4)
1−stearoyl−2−linoleoyl−GPC (18:0/18:2)
1−stearoyl−2−oleoyl−GPC (18:0/18:1)
1−stearoyl−GPC (18:0)
1−stearoyl−GPI (18:0)
2−palmitoleoyl−GPC (16:1)
2−palmitoyl−GPC(16:0)
glycerate
glycerol 3−phosphate
glycerophosphoinositol
glycerophosphorylcholine (GPC)
glycerophosphoserine
serotonin
sphingomyelin (d18:2/14:0, d18:1/14:1)
sphingosine
sphingosine 1−phosphate
21−hydroxypregnenolone disulfate
21−hydroxypregnenolone monosulfate
5alpha−androstan−3alpha,17alpha−diol disulfate
5alpha−androstan−3alpha,17beta−diol disulfate
5alpha−pregnan−diol disulfate
7−hydroxycholesterol (alpha or beta)
androstenediol (3alpha, 17alpha) monosulfate
GlcNAc sulfate conjugate of C21H34O2 steroid
glycochenodeoxycholate glucuronide
isoursodeoxycholate sulfate
pregnen−diol disulfate*
pregnenetriol disulfate*
tetrahydrocortisol sulfate
thyroxine
glycochenodeoxycholate 3−sulfate
glycoursodeoxycholic acid sulfate
Age
70
20
Sex
F
M
Type
Healthy
non-COVID-19
non-Severe
Severe
6
4
2
0
−2
−4
−6
B
mannose
serotonin
sphingosine
1−(1−enyl−palmitoyl)−2−arachidonoyl −GPC (P−16:0/20:4)
kynurenine
choline
bilirubin degradation product
arachidonate (20:4n6)
Relative intensity
Type
Healthy
non-COVID-19
non-Severe
Severe

Figure 5

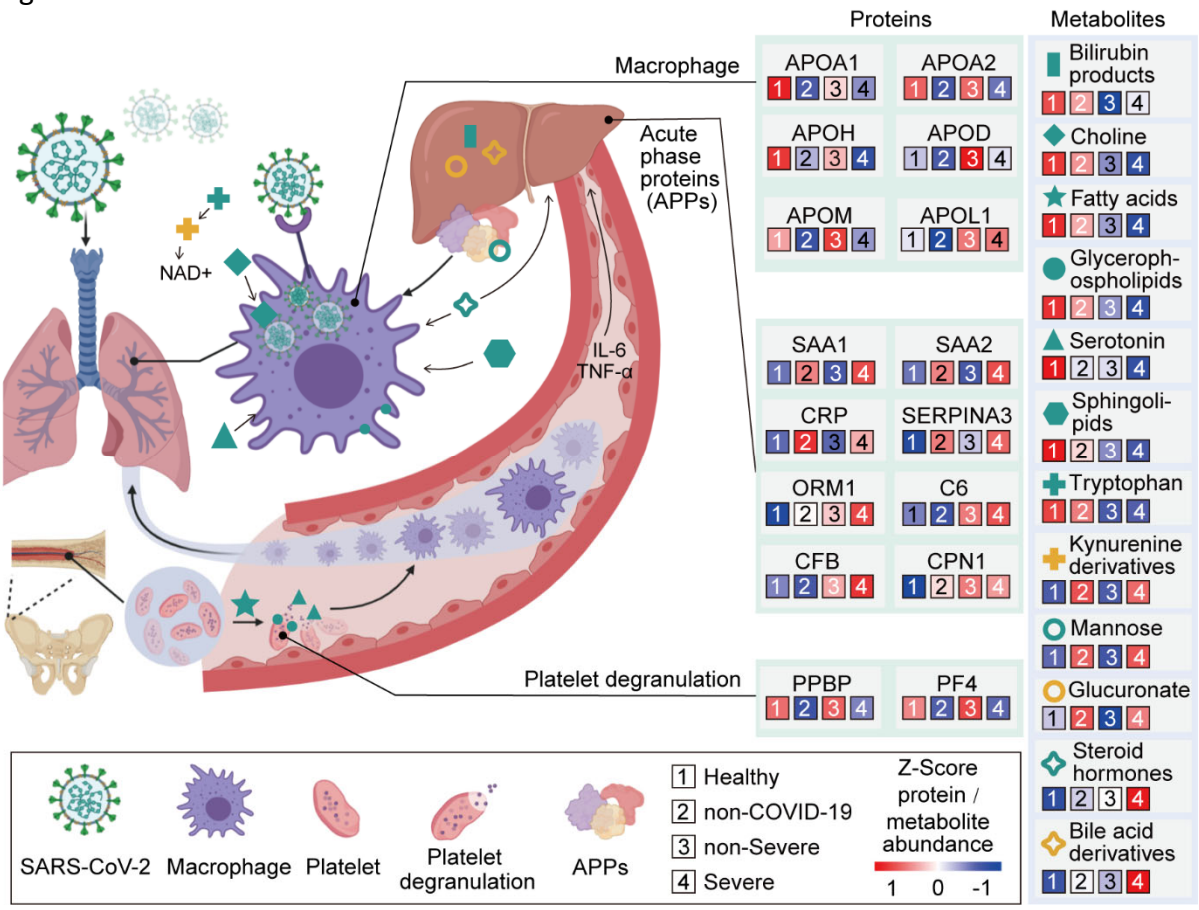
Proteins
Metabolites
Macrophage
Acute phase proteins (APPs)
NAD+
IL-6
TNF-α
Platelet degranulation
APOA1
APOA2
APOH
APOD
APOM
APOL1
SAA1
SAA2
CRP
SERPINA3
ORM1
C6
CFB
CPN1
PPBP
PF4
Bilirubin products
Choline
Fatty acids
Glycerophospholipids
Serotonin
Sphingolipids
Tryptophan
Kynurenine derivatives
Mannose
Glucuronate
Steroid hormones
Bile acid derivatives
SARS-CoV-2
Macrophage
Platelet
Platelet degranulation
APPs
1 Healthy
2 non-COVID-19
3 non-Severe
4 Severe
Z-Score protein / metabolite abundance
1 0 -1

Figure S1

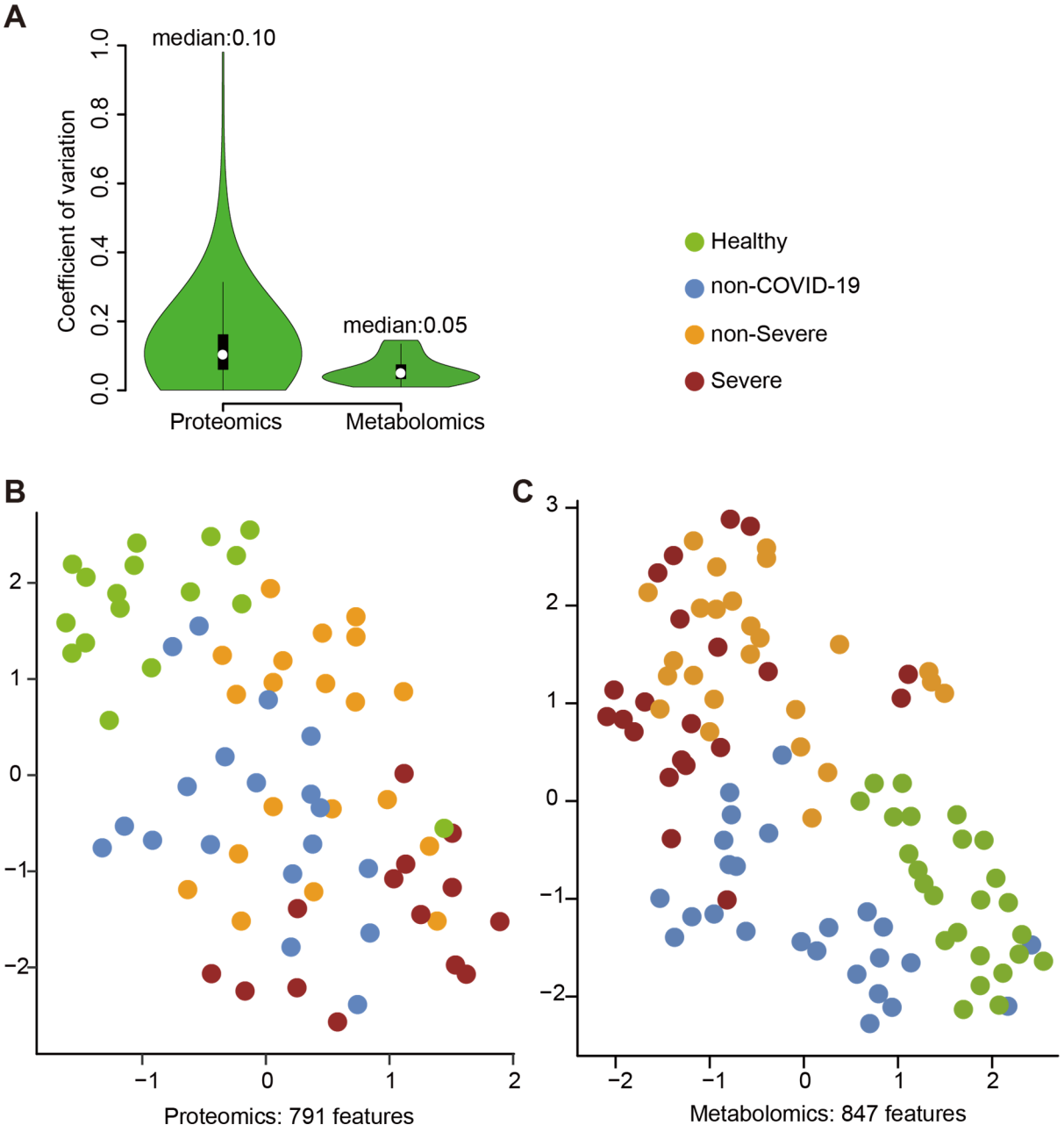
A
median:0.10
median:0.05
Coefficient of variation
0.0
0.2
0.4
0.6
0.8
1.0
Proteomics
Metabolomics
Healthy
non-COVID-19
non-Severe
Severe
B
Proteomics: 791 features
C
Metabolomics: 847 features

Figure S2

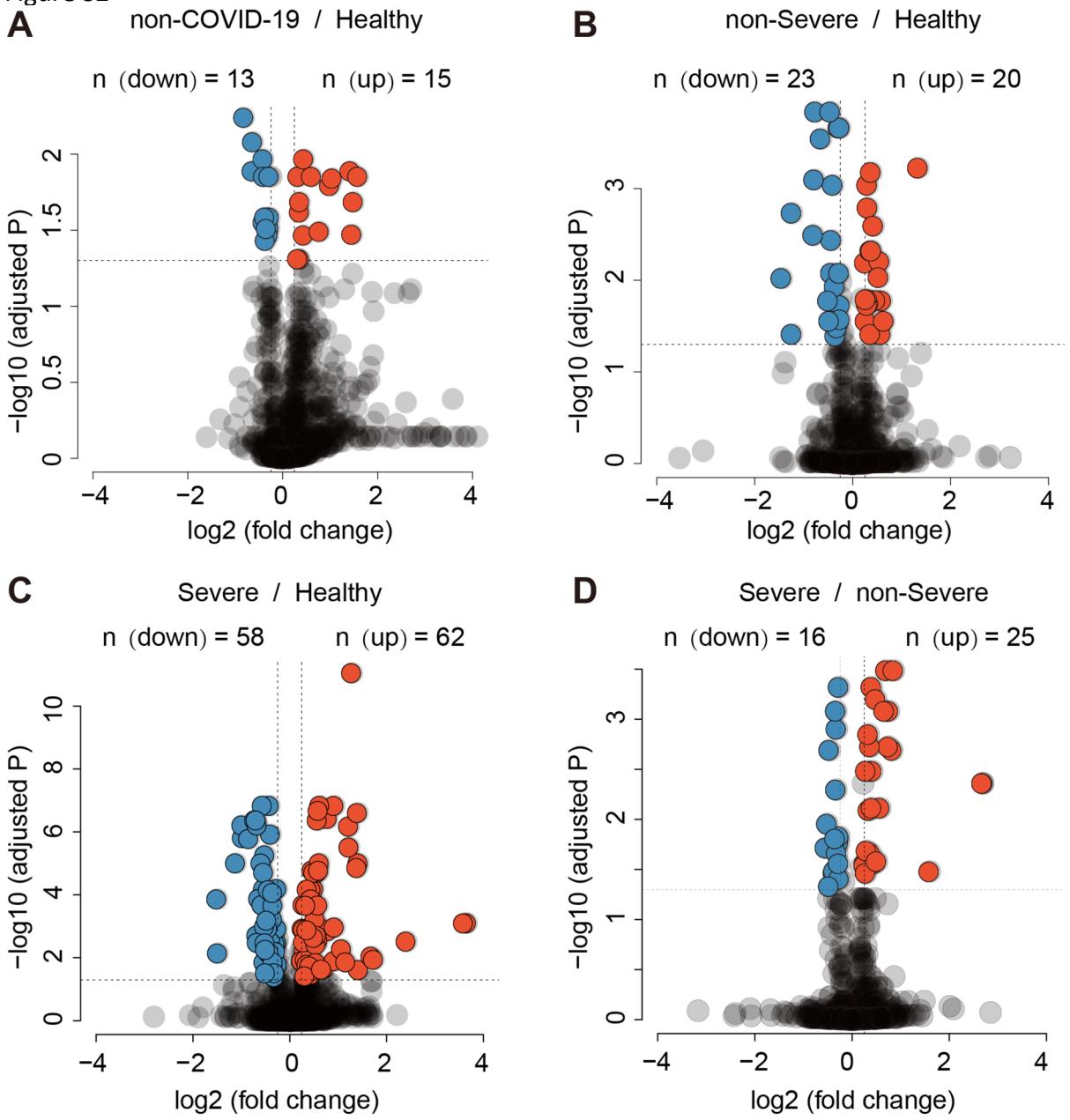
A
non-COVID-19 / Healthy
n (down) = 13
n (up) = 15
−log10 (adjusted P)
log2 (fold change)
B
non-Severe / Healthy
n (down) = 23
n (up) = 20
−log10 (adjusted P)
log2 (fold change)
C
Severe / Healthy
n (down) = 58
n (up) = 62
−log10 (adjusted P)
log2 (fold change)
D
Severe / non-Severe
n (down) = 16
n (up) = 25
−log10 (adjusted P)
log2 (fold change)

Figure S3

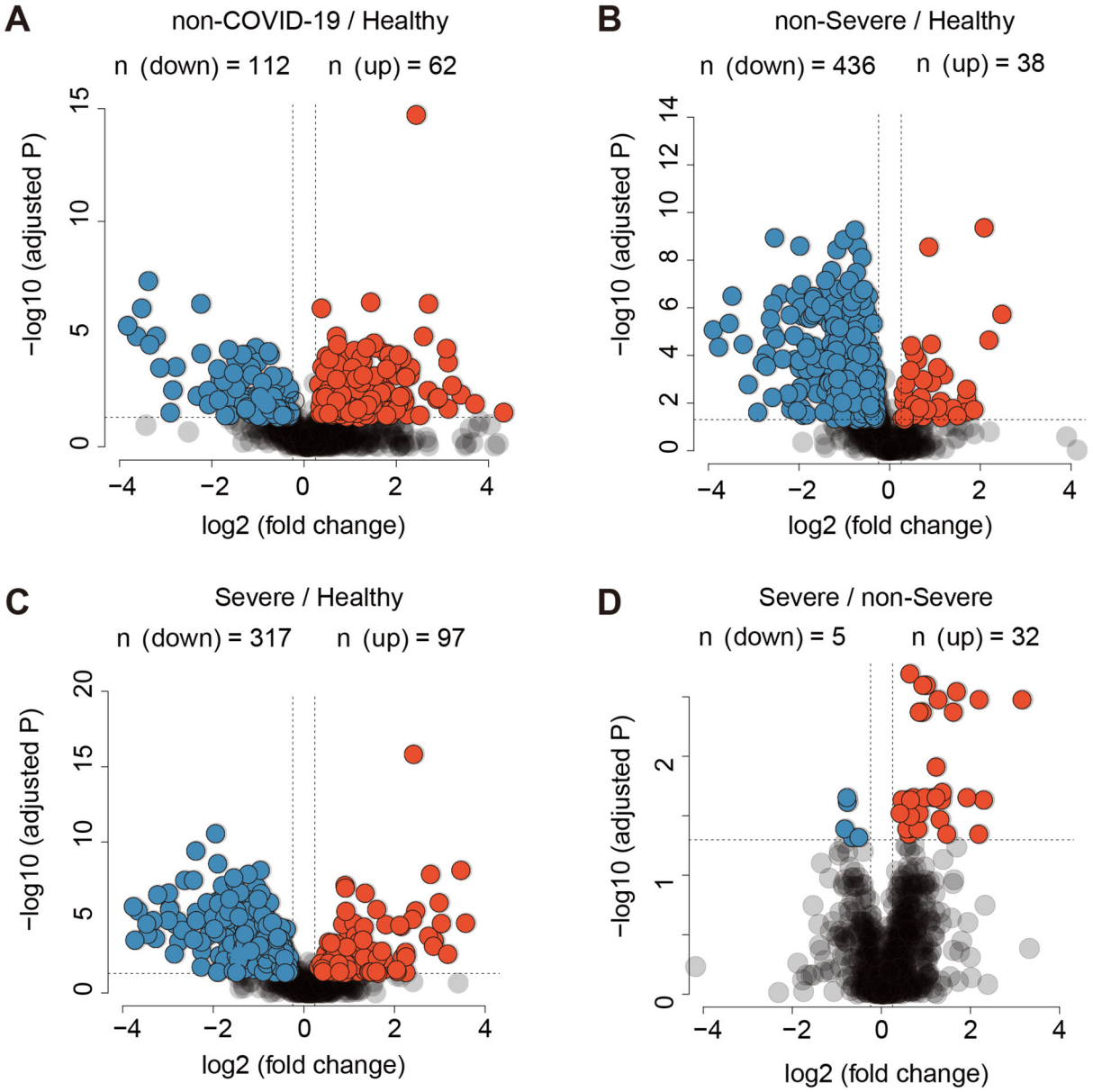
A
non-COVID-19 / Healthy
n (down) = 112
n (up) = 62
−log10 (adjusted P)
log2 (fold change)
B
non-Severe / Healthy
n (down) = 436
n (up) = 38
−log10 (adjusted P)
log2 (fold change)
C
Severe / Healthy
n (down) = 317
n (up) = 97
−log10 (adjusted P)
log2 (fold change)
D
Severe / non-Severe
n (down) = 5
n (up) = 32
−log10 (adjusted P)
log2 (fold change)

Figure S4

A

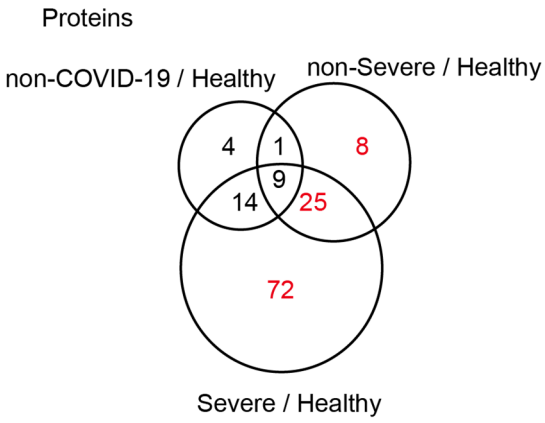
Proteins
non-COVID-19 / Healthy
non-Severe / Healthy
4
1
8
9
14
25
72
Severe / Healthy

B

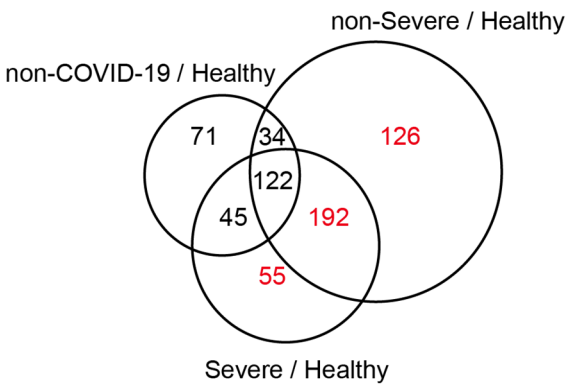
Metabolites
non-Severe / Healthy
non-COVID-19 / Healthy
71
34
126
122
45
192
55
Severe / Healthy

Figure S5

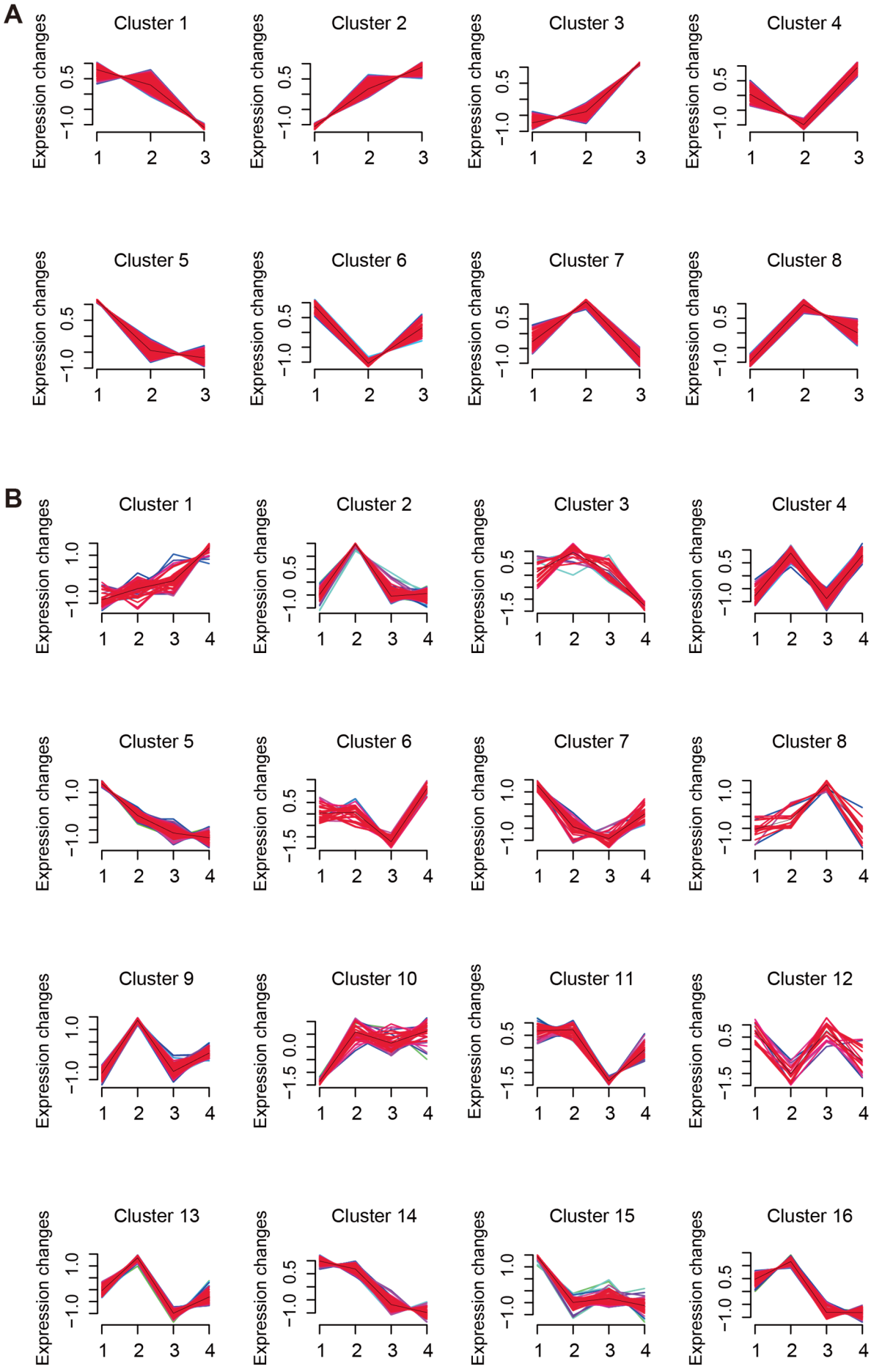
A
Cluster 1
Cluster 2
Cluster 3
Cluster 4
Cluster 5
Cluster 6
Cluster 7
Cluster 8
B
Cluster 1
Cluster 2
Cluster 3
Cluster 4
Cluster 5
Cluster 6
Cluster 7
Cluster 8
Cluster 9
Cluster 10
Cluster 11
Cluster 12
Cluster 13
Cluster 14
Cluster 15
Cluster 16
Expression changes

Figure S6

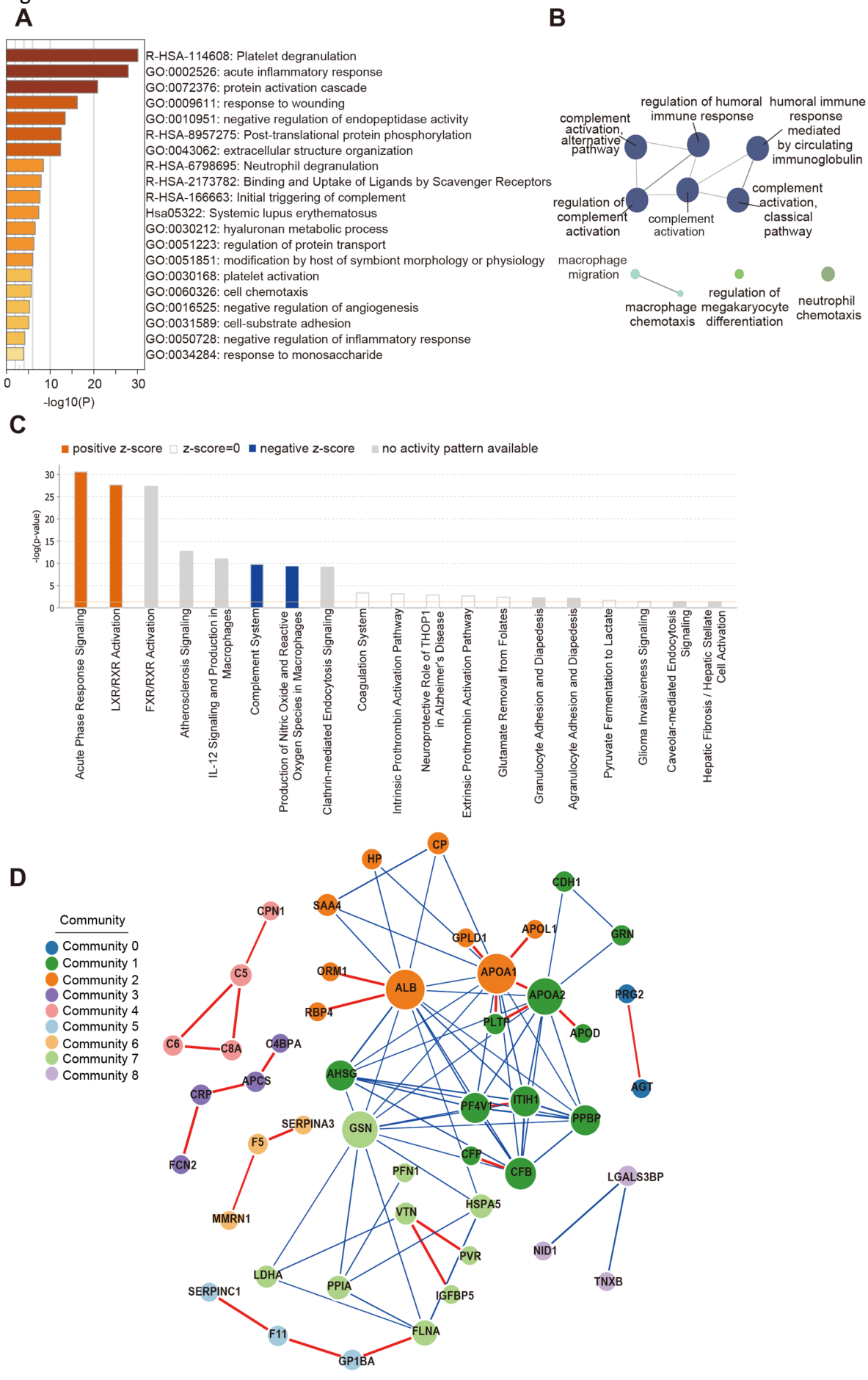
A
R-HSA-114608: Platelet degranulation
GO:0002526: acute inflammatory response
GO:0072376: protein activation cascade
GO:0009611: response to wounding
GO:0010951: negative regulation of endopeptidase activity
R-HSA-8957275: Post-translational protein phosphorylation
GO:0043062: extracellular structure organization
R-HSA-6798695: Neutrophil degranulation
R-HSA-2173782: Binding and Uptake of Ligands by Scavenger Receptors
R-HSA-166663: Initial triggering of complement
Hsa05322: Systemic lupus erythematosus
GO:0030212: hyaluronan metabolic process
GO:0051223: regulation of protein transport
GO:0051851: modification by host of symbiont morphology or physiology
GO:0030168: platelet activation
GO:0060326: cell chemotaxis
GO:0016525: negative regulation of angiogenesis
GO:0031589: cell-substrate adhesion
GO:0050728: negative regulation of inflammatory response
GO:0034284: response to monosaccharide
0
10
20
30
-log10(P)
B
regulation of humoral immune response
humoral immune response mediated by circulating immunoglobulin
complement activation, alternative pathway
regulation of complement activation
complement activation
complement activation, classical pathway
macrophage migration
macrophage chemotaxis
regulation of megakaryocyte differentiation
neutrophil chemotaxis
C
positive z-score
z-score=0
negative z-score
no activity pattern available
-log(p-value)
Acute Phase Response Signaling
LXR/RXR Activation
FXR/RXR Activation
Atherosclerosis Signaling
IL-12 Signaling and Production in Macrophages
Complement System
Production of Nitric Oxide and Reactive Oxygen Species in Macrophages
Clathrin-mediated Endocytosis Signaling
Coagulation System
Intrinsic Prothrombin Activation Pathway
Neuroprotective Role of THOP1 in Alzheimer's Disease
Extrinsic Prothrombin Activation Pathway
Glutamate Removal from Folates
Granulocyte Adhesion and Diapedesis
Agranulocyte Adhesion and Diapedesis
Pyruvate Fermentation to Lactate
Glioma Invasiveness Signaling
Caveolar-mediated Endocytosis Signaling
Hepatic Fibrosis / Hepatic Stellate Cell Activation
D
Community
Community 0
Community 1
Community 2
Community 3
Community 4
Community 5
Community 6
Community 7
Community 8
CP
HP
CDH1
CPN1
SAA4
GPLD1
APOL1
GRN
C5
ORM1
ALB
APOA1
APOA2
PRG2
RBP4
PLTP
APOD
C6
C8A
C4BPA
AHSG
AGT
APCS
CRP
PF4V1
ITIH1
PPBP
SERPINA3
GSN
F5
FCN2
CFP
CFB
PFN1
LGALS3BP
HSPA5
MMRN1
VTN
NID1
PVR
LDHA
TNXB
PPIA
SERPINC1
IGFBP5
FLNA
F11
GP1BA